Measurements of hydroxyl and hydroperoxy radicals during CalNex-LA: Model comparisons and radical budgets

S. M. Griffith, R. F. Hansen, S. Dusanter, V. Michoud, J. B. Gilman, W. C. Kuster, P. R. Veres, M. Graus, J. A. de Gouw, J. Roberts, et al.

AGU PUBLICATIONS

JGR

Journal of Geophysical Research: Atmospheres

RESEARCH ARTICLE
10.1002/2015JD024358

Key Points:
- Measurements of OH and HO2 during CalNex-LA displayed a weekend effect
- Modeled OH and HO2 agreed with measurements after accounting for missing OH reactivity
- Ozone production was VOC limited on the weekdays but NOx limited on the weekends

Supporting Information:
- Supporting Information S1

Correspondence to:
P. S. Stevens,
pstevens@indiana.edu

Citation:
Griffith, S. M., et al. (2016), Measurements of hydroxyl and hydroperoxy radicals during CalNex-LA: Model comparisons and radical budgets, *J. Geophys. Res. Atmos.*, *121*, 4211–4232, doi:10.1002/2015JD024358.

Received 20 OCT 2015
Accepted 25 MAR 2016
Accepted article online 2 APR 2016
Published online 21 APR 2016

Measurements of hydroxyl and hydroperoxy radicals during CalNex-LA: Model comparisons and radical budgets

S. M. Griffith[1,2], R. F. Hansen[3,4], S. Dusanter[1,5,6], V. Michoud[6,7,8], J. B. Gilman[9,10], W. C. Kuster[10], P. R. Veres[9,10], M. Graus[9,10,11], J. A. de Gouw[9,10], J. Roberts[9,10], C. Young[9,10,12], R. Washenfelder[9,10], S. S. Brown[9,10], R. Thalman[13,14], E. Waxman[13], R. Volkamer[13], C. Tsai[15], J. Stutz[15], J. H. Flynn[16], N. Grossberg[16], B. Lefer[16,17], S. L. Alvarez[16], B. Rappenglueck[16], L. H. Mielke[18,19], H. D. Osthoff[18], and P. S. Stevens[1,3]

[1]School of Public and Environmental Affairs, Indiana University, Bloomington, Indiana, USA, [2]Now at Department of Chemistry, Hong Kong University of Science and Technology, Hong Kong, [3]Department of Chemistry, Indiana University, Bloomington, Indiana, USA, [4]Now at School of Chemistry, University of Leeds, Leeds, UK, [5]Mines Douai, SAGE, Douai, France, [6]Université de Lille, Lille, France, [7]LISA/IPSL, Laboratoire Interuniversitaire des Systèmes Atmosphériques, UMR CNRS 7583, Université Paris Est Créteil (UPEC) et Université Paris Diderot (UPD), Créteil, France, [8]Now at Mines Douai, SAGE, Douai, France, [9]Cooperative Institute for Research in Environmental Sciences, University of Colorado Boulder, Boulder, Colorado, USA, [10]Chemical Sciences Division, Earth System Research Laboratory, National Oceanic and Aeronautic Administration, Boulder, Colorado, USA, [11]Now at Institute of Atmospheric and Cryospheric Sciences, Innsbruck University, Innsbruck, Austria, [12]Now at Department of Chemistry, Memorial University of Newfoundland, St. John's, Newfoundland and Labrador, Canada, [13]Department of Chemistry and Biochemistry and CIRES, University of Colorado Boulder, Boulder, Colorado, USA, [14]Now at Department of Chemistry, Snow College, Ephraim, Utah, USA, [15]Department of Atmospheric and Oceanic Sciences, University of California, Los Angeles, California, USA, [16]Department of Earth and Atmospheric Sciences, University of Houston, Houston, Texas, USA, [17]Now at Earth Science Division, NASA Headquarters, Washington, District of Columbia, USA, [18]Department of Chemistry, University of Calgary, Calgary, Alberta, Canada, [19]Now at Department of Chemistry, University of Indianapolis, Indianapolis, Indiana, USA

Abstract Measurements of hydroxyl (OH) and hydroperoxy (HO_2*) radical concentrations were made at the Pasadena ground site during the CalNex-LA 2010 campaign using the laser-induced fluorescence-fluorescence assay by gas expansion technique. The measured concentrations of OH and HO_2* exhibited a distinct weekend effect, with higher radical concentrations observed on the weekends corresponding to lower levels of nitrogen oxides (NO_x). The radical measurements were compared to results from a zero-dimensional model using the Regional Atmospheric Chemical Mechanism-2 constrained by NO_x and other measured trace gases. The chemical model overpredicted measured OH concentrations during the weekends by a factor of approximately 1.4 ± 0.3 (1σ), but the agreement was better during the weekdays (ratio of 1.0 ± 0.2). Model predicted HO_2* concentrations underpredicted by a factor of 1.3 ± 0.2 on the weekends, while measured weekday concentrations were underpredicted by a factor of 3.0 ± 0.5. However, increasing the modeled OH reactivity to match the measured total OH reactivity improved the overall agreement for both OH and HO_2* on all days. A radical budget analysis suggests that photolysis of carbonyls and formaldehyde together accounted for approximately 40% of radical initiation with photolysis of nitrous acid accounting for 30% at the measurement height and ozone photolysis contributing less than 20%. An analysis of the ozone production sensitivity reveals that during the week, ozone production was limited by volatile organic compounds throughout the day during the campaign but NO_x limited during the afternoon on the weekends.

1. Introduction

Hydroxyl (OH) and peroxy (HO_2 and RO_2) radicals play a central role in the chemistry of the atmosphere. The OH radical initiates the oxidation of volatile organic compounds (VOCs) through a series of reactions that convert OH to both HO_2 and organic peroxy radicals (RO_2), which are converted back to OH in the presence of nitrogen oxides ($NO_x = NO + NO_2$). This chemistry results in a fast radical chain that leads to the production of ozone and secondary organic aerosols in the troposphere. Understanding the chemistry of OH, HO_2, and RO_2 radicals (together RO_x) is critical for the development of effective air quality control strategies, as the formation of photochemical pollutants such as ozone, secondary aerosols, peroxides, and organic nitrates can be limited by radical concentrations.

Table 1. Daytime HO_x Measured Versus Model Agreement for Nonwinter Urban Campaigns

Campaign	Date	Location	OH^a (10^6 cm^{-3})	$HO_2{}^a$ (10^8 cm^{-3})	Obs/ModelOH	Obs/ModelHO_2	Comments[b]	References
LAFRE	Sep 1993	Los Angeles, CA, USA	5.0[c]	1.8[c]	0.7	0.6	2 days, midday	*George et al.* [1999]
BERLIOZ	Jul–Aug 1998	Pabstthum, Germany	7.0[d]	4.5[d]	0.5	0.7	1 day;1000–1400 h	*Konrad et al.* [2003]
SOS	Jun–Jul 1999	Nashville, TN, USA	10.0	8.3	1.3	1.6	All points daytime	2003
PUMA	Jun 1999	Birmingham, UK	3.5[e]	1.8[e]	1.7	1.8	All points1100–1500 h	*Emmerson et al.* [2005]
PMTACS	Jun–Aug 2001	New York City, NY, USA	8.8[f]	1.5[f]	1.6[f]	1.8[f]	Campaign median; midday	*Ren et al.* [2003a, 2003b]
MCMA	Apr 2003	Mexico City, Mexico	9[f]	11[f]	1.1[f]	1.4[f]	Campaign median, midday	*Shirley et al.* [2006] and *Sheehy et al.* [2010]
TORCH	Jul–Aug 2003	Essex, UK	2.2	0.8	0.8	0.9	Campaign avg; midday	*Emmerson et al.* [2007]
IMPACT	Jul–Aug 2004	Tokyo, Japan	6.0	1.5	1.2	0.8	All points;0900–1500 h	*Kanaya et al.* [2007]
MILAGRO	Mar 2006	Mexico City, Mexico	4.0	2.0	0.6	1.0	Campaign median; midday	*Dusanter et al.* [2009b]
PRIDE	Jul 2006	Pearl River Delta, China	13.0	13.0	3.0	0.8	Campaign avg; 1100–1500 h	*Lu et al.* [2012]
TRAMP	Aug–Sep 2006	Houston, TX, USA	15	12.5	1.5	1.7	Campaign median; 1130–1730 h	*Chen et al.* [2010]
CARE	Aug–Sep 2006	Beijing, China	8.0	15.0	2.5	1.0	Campaign avg; 1200–1600 h	*Lu et al.* [2013]
SHARP	Apr–May 2009	Houston, TX, USA	8.8	6.3	0.9–1.36	1.2–2.66	Campaign median; daytime	*Ren et al.* [2013] and *Czader et al.* [2013]
MEGAPOLI	July 2009	Paris, France	4.2	1.4[g]	1.1	1.1[g]	All points	*Michoud et al.* [2012]
CalNex-LA	May–Jun 2010	Los Angeles, CA	4.0, 3.5[h]	5.0, 2.0[h]	0.7, 1.0[h]	1.3, 3.4[h]	All points; 0600–2100	This study

[a]Unless otherwise noted, OH and HO_2 concentrations are peak values from campaign mean or median values provided in the reference. Reported HO_2 concentrations may not account for interferences from RO_2 radicals.
[b]Comments provide the temporal details for the obs/model ratio provided in the table.
[c]Values are from the two full days of measurements.
[d]Values are from a single polluted day analyzed in *Konrad et al.* [2003].
[e]Peak OH and HO_2 for PUMA are based on a 4 day average value given in *Emmerson et al.* [2005].
[f]Peak OH and HO_2 for PMTACS and MCMA-2003 are based on revised concentrations given in *Mao et al.* [2010] and obs/model OH and HO_2 corrected based on calibration correction described by *Ren et al.* [2008] and *Mao et al.* [2010].
[g]Value is for $HO_2 + RO_2$.
[h]HO_2 measurements reflect $HO_2{}^*$. Values given are "weekends, weekdays," and peak OH and $HO_2{}^*$ concentrations are from the campaign averages.

Previous campaigns in urban areas focusing on HO_x (OH and HO_2) chemistry (see Table 1) have reported observed daytime OH concentrations that were up to a factor of 2 lower than modeled concentrations [*George et al.,* 1999; *Konrad et al.,* 2003; *Dusanter et al.,* 2009b], while others have reported observed concentrations that were up to a factor of 3 greater than model predictions [*Martinez et al.,* 2003; *Ren et al.,* 2003b; *Emmerson et al.,* 2005; *Chen et al.,* 2010; *Lu et al.,* 2012, 2013]. In contrast, several studies have shown good agreement between observed and modeled concentrations [*Shirley et al.,* 2006; *Emmerson et al.,* 2007; *Kanaya et al.,* 2007; *Sheehy et al.,* 2010; *Ren et al.,* 2013; *Czader et al.,* 2013]. In general, measurements under conditions of higher mixing ratios of NO and high OH radical reactivity appear to be consistent with our understanding of NO_x-VOC chemistry [*Rohrer et al.,* 2014]. On the other hand, measurements of OH in forested environments characterized by low concentrations of NO and high concentrations of biogenic VOCs were generally greater than model predictions [*Rohrer et al.,* 2014]. Several OH radical recycling mechanisms have been proposed to explain the observed discrepancies, including peroxy radical isomerization reactions and an unknown OH recycling process from HO_2 and RO_2 radicals [*Peeters et al.,* 2009, 2014; *Hofzumahaus et al.,* 2009; *Lu et al.,* 2012]. However, recent measurements of OH using the fluorescent assay by gas expansion (FAGE) technique in forested environments characterized by low concentrations of NO have revealed the presence of an unknown interference, possibly from the oxidation of biogenic VOCs, which could explain some of the discrepancies observed in these regions [*Mao et al.,* 2012; *Novelli et al.,* 2014a, 2014b].

For HO_2, daytime models have been in agreement within a factor of 3 with measurements, showing model underpredictions [*Martinez et al.,* 2003; *Ren et al.,* 2003b; *Emmerson et al.,* 2005; *Shirley et al.,* 2006; *Chen et al.,* 2010; *Sheehy et al.,* 2010; *Czader et al.,* 2013], overpredictions [*George et al.,* 1999; *Konrad et al.,* 2003], as well as cases of good agreement [*Emmerson et al.,* 2007; *Kanaya et al.,* 2007; *Dusanter et al.,* 2009b; *Lu et al.,* 2012, 2013; *Ren et al.,* 2013]. Both measurement artifacts and missing chemistry in atmospheric models could lead to the discrepancies observed between measured and model-calculated radical concentrations. It is interesting to note that the HO_x measurements described in Table 1 were performed primarily using the FAGE technique, which, as discussed above, might suffer from interferences for both OH [*Mao et al.,* 2012; *Griffith et al.,* 2013; *Novelli et al.,* 2014a, 2014b; *Fuchs et al.,* 2016] and HO_2 [*Fuchs et al.,* 2011; *Ren et al.,* 2012; *Griffith et al.,* 2013; *Whalley et al.,* 2013]. It is not clear to what extent these interferences have impacted the model-measurement agreements discussed above.

An underprediction of HO_x radical concentrations could result from either a missing or underestimated source of radicals in the model or an overestimation of a radical sink. Radical

budget analyses made for the studies cited above have highlighted the importance of the photolysis of nitrous acid (HONO) and carbonyls as well as the ozonolysis of alkenes as important sources of radicals in polluted environments [*Shirley et al.,* 2006; *Dusanter et al.,* 2009b; *Volkamer et al.,* 2010; *Stone et al.,* 2012]. Additional field studies including experimental measurements of these species are needed to better assess the contribution of these radical sources to the oxidative capacity of the atmosphere.

Model overpredictions of HO_x radical concentrations might be indicative of missing or underestimated radical sinks in the model, in addition to an overestimation of a radical source. The likely presence of thousands of volatile organic compounds in the atmosphere [*Goldstein and Galbally*, 2007] makes exhaustive measurements very challenging. In this context, measurements of total OH reactivity can be used to investigate the potential for missing loss routes in the model [*Martinez et al.,* 2003; *Ren et al.,* 2003a, 2003b; *Di Carlo et al.,* 2004*; Shirley et al.,* 2006]. This is particularly important in urban environments that might contain a complex set of primary anthropogenic and biogenic VOCs and multigenerational oxidation products in addition to contributions from organic aerosol evaporation [*Sheehy et al.,* 2010]. The determination of "missing" OH reactivity by comparing OH reactivity values calculated from trace gas measurements to measured values can be an important constraint for reconciling models with measurements [*Ren et al.,* 2003b; *Shirley et al.,* 2006].

An incomplete understanding of HO_x radical propagation and chain length might also lead to discrepancies between models and measurements [*Sheehy et al.,* 2010]. Measurements of the HO_2/OH ratio have been used as a metric to investigate the propagation chemistry in the model as this ratio does not depend on radical initiation and termination routes. Modeled HO_2/OH ratios have been shown to be in reasonable agreement with measurements at NO mixing ratios close to 1–2 ppbv, but a significant difference is observed at higher NO mixing ratios (up to a factor 10 at 100 ppbv of NO) [*Shirley et al.,* 2006; *Dusanter et al.,* 2009b; *Chen et al.,* 2010; *Ren et al.,* 2013]. This NO-dependent discrepancy could indicate either an NO-dependent measurement artifact, segregation of radicals due to inhomogeneous mixing near emission sources [*Kanaya et al.*, 2007; *Dusanter et al.,* 2009b; *Dlugi et al.,* 2010], or a significant misunderstanding about radical cycling under high NO conditions and could have important implications for the reliability of models in assessing ozone production in urban areas [*Dusanter et al.,* 2009b].

Since the observed discrepancies between measured and model-calculated radical concentrations could be due to a combination of measurement artifacts and incomplete chemistry in atmospheric models, additional measurements of HO_x radicals together with investigations of potential instrumental artifacts are needed to test our understanding of the fast photochemistry in urban areas. This study presents measurements of HO_x concentrations made during the 2010 California Research at the Nexus of Air Quality and Climate Change measurement campaign in Los Angeles (CalNex-LA). The measurements are compared to the results of a zero-dimensional box model to test the ability of the model to reproduce observed radical concentrations. Differences between the observed and modeled concentrations, radical budgets, and ozone production regimes are examined and compared to the results from other urban campaigns.

2. Experimental Methods

2.1. Measurement Site and Supporting Measurements

The CalNex 2010 campaign was a field project designed to improve the scientific understanding needed to support effective emission control strategies that address both issues of air quality and climate change. An overview of the entire CalNex campaign can be found in *Ryerson et al.* [2013], with a comprehensive listing of all the platforms, site locations, and individual measurements, including a list of all the instruments at the CalNex ground site in the Los Angeles air basin. The CalNex-LA site was located at the campus of the California Institute of Technology in Pasadena approximately 18 km northeast of downtown Los Angeles and generally receives onshore sea-breeze driven airflow from the southwest and downtown Los Angeles during the daytime [*Washenfelder et al.,* 2011; *Ryerson et al.,* 2013]. In addition, the ground site is also impacted by local emissions of VOCs and NO_x from traffic and other anthropogenic activities. Measurements at this site occurred between 15 May and 16 June 2010.

Two 10 m towers were installed at the CalNex-LA site, one for gas-phase measurements and one for aerosol-phase measurements. A suite of measurements shown in Table 2 contributed to this modeling analysis. The NOAA tropospheric chemistry group measured C2–C10 nonmethane hydrocarbons (NMHCs) using gas

Table 2. Supporting Measurements From the CalNex-LA Site Used to Constrain the Model

Measurement	Reference	Technique	Sample Interval	Accuracy at High S/N	Precision at Low S/N
C2–C10 NMHCs	*Kuster et al.* [2004]	GC-MS	30 min	20%	10 pptv
O_3	*Lefer et al.* [2010]	UV absorption	1 min	4%	500 pptv, 4%
NO, NO_2, NO_Y	*Drummond et al.* [1985], *Pollack et al.* [2010], and *Williams et al.* [1988]	Gas-phase chemiluminescence	1 min	4% NO6% NO_2 4% NO_Y	20 pptv NO50 pptv NO_2 40 pptv NO_Y, 4%
SO_2	*Luke* [1997]	Pulsed UV fluorescence	10 min	15%	200 pptv
CO	*Gerbig et al.* [1999] and *Newman et al.* [2013]	Vacuum ultraviolet resonance fluorescence spectroscopy	10 s	4%	0.2 ppbv
CHOCHO and HONO	*Washenfelder et al.* [2008]	Incoherent broadband cavity-enhanced absorption spectrometry	10 min	15% and 30%	13 pptv and 52 pptv
HNO_3, HONO, and Org. Acids	*Veres et al.* [2008]	Negative-ion proton transfer chemical ionization mass spectrometry	1 min	30%	40 pptv
PAN	*Mielke et al.* [2013]	I^- CIMS	25 s	30%	3%
HCHO	*Rappenglück et al.* [2010] and *Warneke et al.* [2011, 2013]	Liquid-phase fluorescence using Hantzsch reaction	1 min	10%	60 pptv
Photolysis Frequencies	*Shetter and Muller* [1999] and *Cantrell et al.* [2003]	Spectrally resolved radiometry	30 s	15% (JNO_2) 30% ($JO(^1D)$)	$0.3 \times 10^{-4}\ s^{-1}$ (JNO_2) $0.3 \times 10^{-7}\ s^{-1}$ ($JO(^1D)$) < 1%

chromatography/mass spectrometry (GC/MS) [*Kuster et al.,* 2004], nitrous acid, and glyoxal using incoherent broadBand cavity enhanced absorption spectroscopy [*Washenfelder et al.,* 2008, 2011] and nitrous acid, nitric acid, and organic acids by negative-ion-proton transfer chemical ionization mass spectrometry (CIMS) [*Veres et al.,* 2008; *Roberts et al.,* 2010; *Veres et al.,* 2011] in addition to meteorological parameters.

The University of Houston group measured NO and NO_2 by gas-phase chemiluminescence with a blue light converter for NO_2 [*Lefer et al.,* 2010], SO_2 by pulsed UV fluorescence [*Luke,* 1997], CO by vacuum UV resonance fluorescence spectroscopy [*Gerbig et al.,* 1999; *Newman et al.,* 2013], formaldehyde by liquid-phase fluorescence [*Rappenglück et al.,* 2010; *Warneke et al.,* 2011, 2013], and photolysis frequencies by spectral radiometry [*Shetter and Muller*, 1999]. The University of Calgary group measured peroxyacetyl nitrate (PAN) and peroxypropionyl nitrate (PPN) by CIMS [*Mielke et al.,* 2011, 2013]. In addition, measurements of formaldehyde made by differential optical absorption spectrometry (DOAS) by the University of California Los Angeles group [*Wong et al.,* 2012] and measurements of nitrogen dioxide made by cavity enhanced-DOAS by the University of Colorado group [*Thalman and Volkamer*, 2010; *Knote et al.,* 2014] were used for a portion of the analysis. Total hydroxyl radical reactivity was measured using a turbulent flow tube reactor [*Hansen et al.,* 2014; Hansen et al., in preparation]. In this technique, OH radicals were produced in a movable injector by the photolysis of water vapor, and decays of OH reflecting the reactivity with ambient air were measured as a function of reaction time using laser-induced fluorescence techniques. The instrument was calibrated by measuring the reactivity of several compounds with well-known rate constants [*Hansen et al.,* 2014]. Further details about these measurements are given in the supporting information.

2.2. HO_x Radical Measurements

OH and HO_2 radical concentrations were measured using the laser-induced fluorescence-fluorescence assay by gas expansion (LIF-FAGE) technique. The FAGE technique detects OH by laser-induced fluorescence after expansion of ambient air into a low-pressure chamber, enhancing the OH fluorescence lifetime and allowing temporal filtering of the OH fluorescence from laser scatter [*Heard and Pilling*, 2003; *Stone et al.,* 2012]. The Indiana University FAGE (IU-FAGE) instrument has been described in detail elsewhere [*Dusanter et al.,* 2008, 2009a; *Griffith et al.,* 2013], and only a brief description is given here, along with updates that were unique for the CalNex-LA campaign.

The IU-FAGE laser system used in this study consisted of a Spectra Physics Navigator II YHP40-532Q diode-pumped Nd:YAG laser that produces approximately 5.5 W of radiation at 532 nm at a repetition

rate of 5 kHz. This laser pumped a Lambda Physik Scanmate 1 dye laser (Rhodamine 640, 0.25 g L^{-1} in isopropanol) that produced tunable radiation around 616 nm, which was frequency doubled to generate 2 to −20 mW of laser power at 308 nm. OH radicals were excited using the $Q_1(3)$ line of the $A^2\Sigma^+(v'=0) \leftarrow X^2\Pi(v''=0)$ transition, and a reference cell, where OH radicals were produced by thermal dissociation of water vapor, was used to ensure maximum overlap of the laser with the OH transition [*Dusanter et al.,* 2009a].

After exiting the dye laser, the laser beam was focused onto the entrance of a 12 m optical fiber to transmit the radiation to the sampling cell. The net OH fluorescence signal was determined by successive modulation cycles during which the laser wavelength was successively tuned on resonance with the OH transition to measure the OH fluorescence, and off resonance to measure a background signal due to solar and laser scatter that is subtracted. Elevated background signals were not observed for either "off-line" position surrounding the $Q_1(3)$ transition while cycling during HO_x measurements, suggesting that spectral interferences were negligible during the CalNex-LA campaign.

The sampling cell was placed at the top of the 10 m tower, and ambient air was expanded into the detection region through a 0.6 mm inlet. The pressure in the cell was maintained at 4.0 ± 0.1 torr (~5.3 ± 0.1 hPa) using two scroll pumps (Edwards, XDS35i) connected in parallel. A Teflon loop located directly below the inlet allowed for the intermittent addition of NO to convert ambient HO_2 to OH through the fast $HO_2 + NO \rightarrow OH + NO_2$ reaction, allowing for indirect measurements of HO_2. The optimum NO flow (approximately 1 cm^3 min^{-1}, 3×10^{13} cm^{-3}) used to convert the HO_2 radicals before the detection axis was a trade-off between the conversion of HO_2 into OH and the removal of OH by reaction with NO. The fraction of HO_2 (C_{HO2}) converted into OH was measured during calibration experiments [*Dusanter et al.,* 2008, 2009a]. The airstream passed through the central region of the sampling cell where the laser beam was reflected 24 times in a multipass cell (White configuration). The OH fluorescence was collected at right angles to both the airstream and the laser beam and detected using a microchannel plate detector (Hamamatsu, R5916U) and a gated detection scheme. The laser power was continuously monitored by a photodiode mounted at the exit of the multipass cell. The stability of the laser power entering the detection cell was improved compared to previous deployments of IU-FAGE by heating and flushing with N_2 the outside of the entrance window of the detection axis, which was also covered by an insulated aluminum enclosure, preventing condensation from forming on the window or shifting of the optical fiber mount.

IU-FAGE calibrations during CalNex-LA were performed using the UV water photolysis method [*Dusanter et al.,* 2008] and were made every 3 days to track the sensitivity of the instrument. For these calibrations, ultrazero air was sent through a humidifier at the base of the tower and delivered at 50 L min^{-1} to the HO_x calibrator [*Dusanter et al.,* 2008]. Uncertainties associated with the UV water photolysis calibrator used for IU-FAGE have been described previously [*Dusanter et al.,* 2008; *Griffith et al.,* 2013] and are estimated to be 18% (1σ) for both OH and HO_2. The typical OH detection limit for IU-FAGE during CalNex-LA was 3.4×10^5 cm^{-3} (S/N = 1, 15 min average).

2.3. OH Measurement Interference

The IU-FAGE instrument was previously found to be sensitive toward interferences due to laser photolysis of ozone in the sampling cell (R1) and the subsequent reaction of $O(^1D)$ with water (R2) [*Griffith et al.,* 2013]:

(R1) $$O_3 + h\nu \rightarrow O(^1D) + O_2$$

(R2) $$O(^1D) + H_2O \rightarrow OH + OH$$

Although this laser-generated interference is smaller in other LIF-FAGE instruments [*Ren et al.,* 2004], this interference in the IU-FAGE instrument could be due to double pulsing of the same airmass in the multipass cell in combination with high laser fluence and potential recirculation inside the detection axis. During the CalNex-LA campaign, this interference was calibrated by measuring the laser-generated OH signal as a function of both water vapor and ozone concentrations and found to be equivalent to 7500 ($1\sigma = 1000$) molecule cm^{-3} of OH when normalized to 1 ppbv of O_3, 1% of water, and 1 mW of laser power (supporting information). To minimize this interference while maintaining a reasonable limit of detection for OH, the laser power entering the detection cell was kept between 2 and 3 mW using neutral-density filters, resulting in an average interference signal at noon that was approximately 33% of the total signal (see supporting information).

To quantify this interference and any other potential interferences during ambient measurements of OH, an automated injector was designed to add perfluoropropylene (C_3F_6) above the sampling nozzle to chemically remove ambient OH [*Griffith et al.,* 2013]. Measurements of net OH signals during the C_3F_6 addition reflect non-ambient OH produced inside the detection cell and were subtracted from the net OH signals acquired when C_3F_6 was not added. The measurement time sequence used for OH measurements was 40 min of ambient OH + interferences (no addition of C_3F_6) followed by 20 min of interference measurements (C_3F_6 addition). Measurement and subtraction of the laser-generated interference reduced the overall performance of the instrument, resulting in a limit of detection of 4.4×10^5 cm^{-3} (S/N = 1, 15 min average).

The measured interference was compared to that calculated from the calibrated O_3/water laser-generated interference (reactions (R1) and (R2)) using ambient measurements of ozone, water, and laser power and was found to be consistent with the laser-generated interference expected from reactions (R1) and (R2) throughout the campaign, as the calculated and measured interference agreed to within their combined uncertainty (supporting information). This is in contrast to recent measurements in forested environments [*Mao et al.,* 2012; *Novelli et al.,* 2014a, 2014b]. However, recent laboratory measurements of the OH radical yield produced from the ozonolysis of several biogenic alkenes suggests that under high ozone and alkene concentrations the IU-FAGE instrument is sensitive to an interference associated with certain biogenic monoterpenes such as α and β pinene (Sigler et al., in preparation). The absence of an unknown interference during CalNex-LA is likely due to lower concentrations of these biogenic compounds compared to forested areas where interferences have been previously observed.

2.4. HO_2 Measurement Interference

As mentioned previously, HO_2 radicals are detected indirectly by converting HO_2 to OH using the $HO_2 + NO \rightarrow OH + NO_2$ reaction. However, it has recently been established that FAGE instruments measuring HO_2 by chemical conversion to OH with NO may be prone to potential interferences from organic peroxy radicals [*Fuchs et al.,* 2011; *Ren et al.,* 2012; *Griffith et al.,* 2013]. In particular, hydroxy peroxy radicals derived from alkene oxidation can efficiently interfere with the HO_2 measurement by first converting to an alkoxy radical by reaction with NO (R3). The β-hydroxy alkoxy radicals quickly decompose, and the resulting hydroxy alkyl radical can react with O_2 to form HO_2 ((R4) and (R5)) fast enough even with the reduced oxygen concentration inside the FAGE cell and the short reaction time between NO addition to LIF detection:

(R3) $$HORO_2 + NO \rightarrow HORO + NO_2$$

(R4) $$HORO \xrightarrow{decomp} HOR' + R''O$$

(R5) $$HOR' \xrightarrow{O_2} R'O + HO_2$$

As a result, addition of NO to the sampling cell can lead to the conversion of both HO_2 and a fraction of organic peroxy radicals to OH and reflect concentrations of $HO_2^* = HO_2 + \sum \alpha_i RO_{2i}$. The detection efficiency (α) has been determined for several organic peroxy radicals during laboratory calibrations. *Griffith et al.* [2013] detailed the performance of IU-FAGE for the HO_2 measurement during two campaigns in a forest environment where isoprene peroxy radicals were the dominant organic peroxy radical leading to an interference. However, during CalNex, the composition of RO_2 contributing to HO_2^* in IU-FAGE included a variety of both biogenic and anthropogenic peroxy radicals. Thus, α values have been carefully determined experimentally or were estimated for each peroxy radical in order to compare the measured HO_2^* concentrations with the model. Further details of the characterization of the HO_2 interference for the IU-FAGE instrument will be provided in a forthcoming paper (Lew et al., in preparation). The precision for the HO_2^* measurement does not depend on the RO_2 interference and results in a limit of detection for HO_2^* of 2×10^7 cm^{-3} (S/N = 1, 30 s averaging time). However, the HO_2^* modeling uncertainty is impacted by the peroxy radical interference, which is estimated to contribute to approximately 30% of the measured HO_2^* concentration on average (see below).

2.5. Modeling Using the Regional Atmospheric Chemistry Mechanism

For this analysis, the Regional Atmospheric Chemical Mechanism version 2 (RACM2) [*Goliff et al.,* 2013] was used to simulate HO_x radical concentrations at the CalNex-LA site using a 0-D box model constrained by measured concentrations of long-lived species. The RACM2 mechanism was used to model both daily and campaign-averaged concentrations of OH and HO_2^*. Dry deposition rates were constrained by the measured

Table 3. RO_2 Detection Efficiencies for the Modeling Surrogates in the Condensed Mechanism

Measured and Estimated RO_2 Detection Efficiency in IU-FAGE	RACM2 Category	Parent VOC
$\alpha = 1.00 \pm 0.5$	OLTP, OLIP, APIP, LIMP, UALP	Olefins, Monoterpenes[a]
$\alpha = 0.80 \pm 0.2$	BALP, BAL1, BAL2, BENP, ETEP, ISOP, MACP, MCP, MVKP, TLP1, TOLP, TR2, XY2, XYL1, XYLP, XYO2, XYOP, PER1, PER2	Isoprene, Aromatics, Methyl vinyl ketone,[a] Methacrolein[a]
$\alpha = 0.60 \pm 0.3$	HC8P	C8–C10 alkanes[a]
$\alpha = 0.30 \pm 0.15$	HC5P	C5–C7 alkanes
$\alpha = 0.15 \pm 0.08$	HC3P, RCO3	C3–C4 alkanes
$\alpha = 0.07 \pm 0.04$	CH3O2, ETHP, ACTP, KETP, MEKP, ACO3, ORAP	Methane, Ethane, Acetone[a]

[a]Estimated from relative difference of measured RO_2 detection efficiencies in IU-FAGE and those reported in *Fuchs et al.* [2011] (see text).

boundary layer height [*Haman et al.,* 2012], and deposition velocities were modeled similarly to that described by *Michoud et al.* [2012] based on recommendations from *Derwent* [1996] for HNO_3 (2.0 cm s^{-1}) and PANs (0.2 cm s^{-1}). Recommendations from *Brasseur et al.* [1998] were used for aldehydes (0.33 cm s^{-1}), H_2O_2 (1.1 cm s^{-1}), nonacyl organic nitrates (1.1 cm s^{-1}), and organic peroxides (0.55 cm s^{-1}). Additional physical constraints to simulate dilution were tested in the model but only had a minimal impact and were not included in the modeling scenarios presented here (supporting information). The differential equations generated from the chemical mechanism were integrated using the FACSIMILE solver (MCPA Software) and processed through a 5 day spin-up to generate unmeasured secondary species in the model [*Michoud et al.,* 2012]. Each spin-up day was split into 15 min data points, with the model constraints reinitialized every 10 s to ensure constant concentrations over the integration time for the measured long-lived species.

To compare the measured HO_2* with the model, the modeled HO_2* was determined from the modeled HO_2 and RO_2 concentrations and the experimentally derived detection efficiencies (α) using the following equation:

$$HO_2^* = HO_2 + \sum \alpha_i RO_{2i} \quad (1)$$

Here the individual RO_2 species were represented by the different peroxy radical categories in the RACM2 model. All of the RACM2 peroxy radical categories used in determining the modeled HO_2* concentrations from equation (R1) with their corresponding conversion efficiencies under the operating conditions of IU-FAGE during CalNex-LA are listed in Table 3 and are described in the supporting information. For example, experimental detection efficiencies for peroxy radicals derived from isoprene (RACM2 category ISOP) were found to be approximately $\alpha = 0.80 \pm 0.14$, and this detection efficiency was used for several similar RACM2 peroxy radical categories (Table 3 and supporting information). Smaller alkanes such as propane (C3–C4) were found to have conversion efficiencies of approximately $\alpha = 0.15 \pm 0.04$, and this detection efficiency was used for RACM2 peroxy radical categories from alkanes (HC3P). These results are similar to those found for other FAGE instruments [*Fuchs et al.,* 2011; *Whalley et al.,* 2013]. Conversion efficiencies for other RO_2 radicals were estimated based on measurements in our laboratory and those reported in *Fuchs et al.* [2011] (Table 3 and supporting information).

Uncertainties associated with modeled HO_x concentrations were calculated from Monte Carlo simulations using rate constants and measured constraint concentrations that were randomly selected from their uncertainty distributions [*Carslaw et al.*, 1999, 2001; *Griffith et al.,* 2013]. All of the individual model points at 8 A.M. (NO peak on the weekend, local time), 3 P.M., and 1 A.M. (nighttime) were simulated 600 times each with constraint and rate constant values from the uncertainty distribution, resulting in an uncertainty (relative standard deviation) on average of 22% for OH and 35% for HO_2* (1σ). Further discussion of the model uncertainty that details the most sensitive parameters and compares to other reported model uncertainties can be found in the supporting information.

3. Results

3.1. Daily OH and HO_2* Measurements and Model Results

Figure 1 shows the daily measurements of HO_x concentrations made during the campaign, while Figure 2 shows the daily measurements of $J(O^1D)$, NO_x, NO, and ozone. Measured OH concentrations correlated well

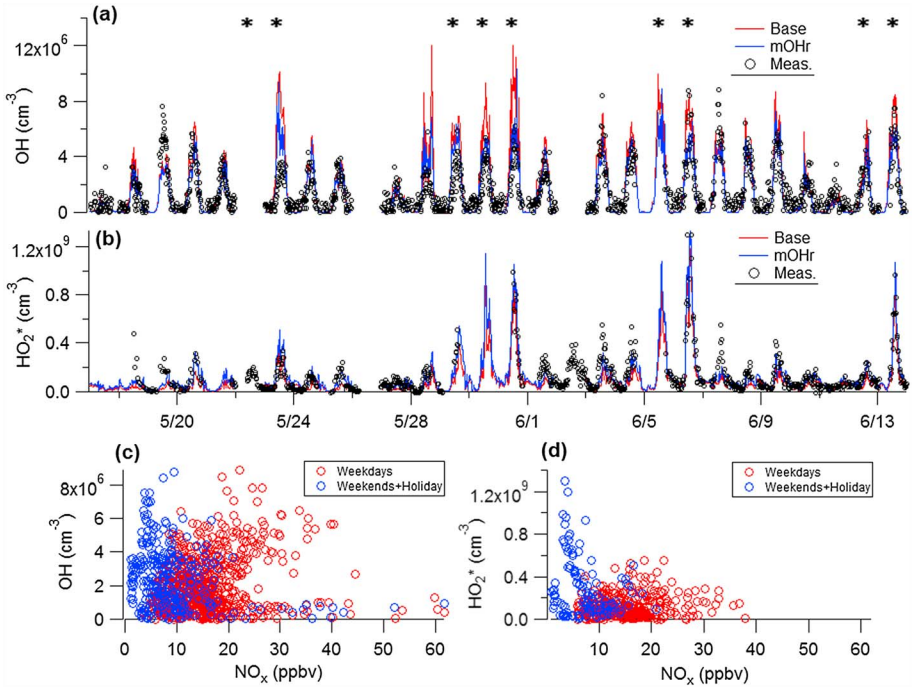

Figure 1. (a) Daily OH measurements (black) compared to RACM2 OH base model (red) and mOHr model (blue), with asterisks indicating the weekends and holiday. (b) The daily HO_2* measurements (black) compared to RACM2 HO_2* base model (red) and mOHr model (blue). Times are PDT. (c and d) The OH and HO_2* measurements as a function of NO_x binned for the weekdays (red circles) and the weekend + holiday (blue circles).

with J(O^1D) similar to previous observations at rural, marine, and urban sites [*Rohrer and Berresheim*, 2006; *Lu et al.,* 2013] (supporting information). Maximum OH and HO_2* concentrations ranged from approximately $(1.5–9)\times10^6\,cm^{-3}$ to $(0.8–10)\times10^8\,cm^{-3}$, respectively. The measured HO_2* concentrations showed a distinct weekend effect, with weekend and Memorial Day holiday measurements of HO_2* (denoted by asterisk in Figure 1) that were significantly higher than the weekday measurements by up to a factor of 10, reflecting the low values of NO observed on the weekend and holidays (less than 4 ppbv on average) compared to that observed during the week (greater than 4 ppb on average), although differences in temperature and photolysis rates between the weekends and the weekdays might also contribute to the different radical concentrations observed on these days. Figure 1 also shows the measurements of OH and HO_2* as a function of NO_x and binned over the weekdays and weekends + holiday, illustrating the NO_x dependence of HO_x. Although differences in VOC concentrations will impact this relationship, it is clear from these plots that the majority of the high concentrations of HO_2* occurred on the weekends when NO_x was less than approximately 4–5 ppbv.

These concentrations of OH and HO_2* are similar to that observed previously by *George et al.* [1999] under clear-sky conditions in the Los Angeles air basin as well as the summertime values reported by *Emmerson et al.* [2005] in Birmingham, UK, and *Kanaya et al.* [2007] in Tokyo even under different ambient conditions. However, results from a number of urban campaigns show distinctly higher OH and HO_2 concentrations than observed during CalNex-LA (Table 1), with maximum values above $1\times10^7\,cm^{-3}$ and $1\times10^9\,cm^{-3}$, for OH and HO_2, respectively, observed on many days [*Martinez et al.,* 2003; *Shirley et al.,* 2006; *Lu et al.,* 2012, 2013]. Other campaigns report higher measured ranges of OH concentrations ($>1\times10^7\,cm^{-3}$) with measured HO_2 concentrations that were similar to that observed during CalNex-LA [*Ren et al.,* 2003a, 2003b; *Dusanter et al.,* 2009a, 2009b; *Ren et al.,* 2013] (Table 1).

Modeled RACM2 (red) OH concentrations are shown in Figure 1 alongside measured OH values. Both the diurnal and the day-to-day variations of OH are well reproduced by the model. However, the modeled OH concentrations during the lower NO_x conditions observed on the weekend days and the holiday consistently overpredict the measured OH values in the first half of the campaign, with better agreement over the last two weekends. Figure 1 also compares daily HO_2* measurements with RACM2 modeled HO_2* (red). Based on the

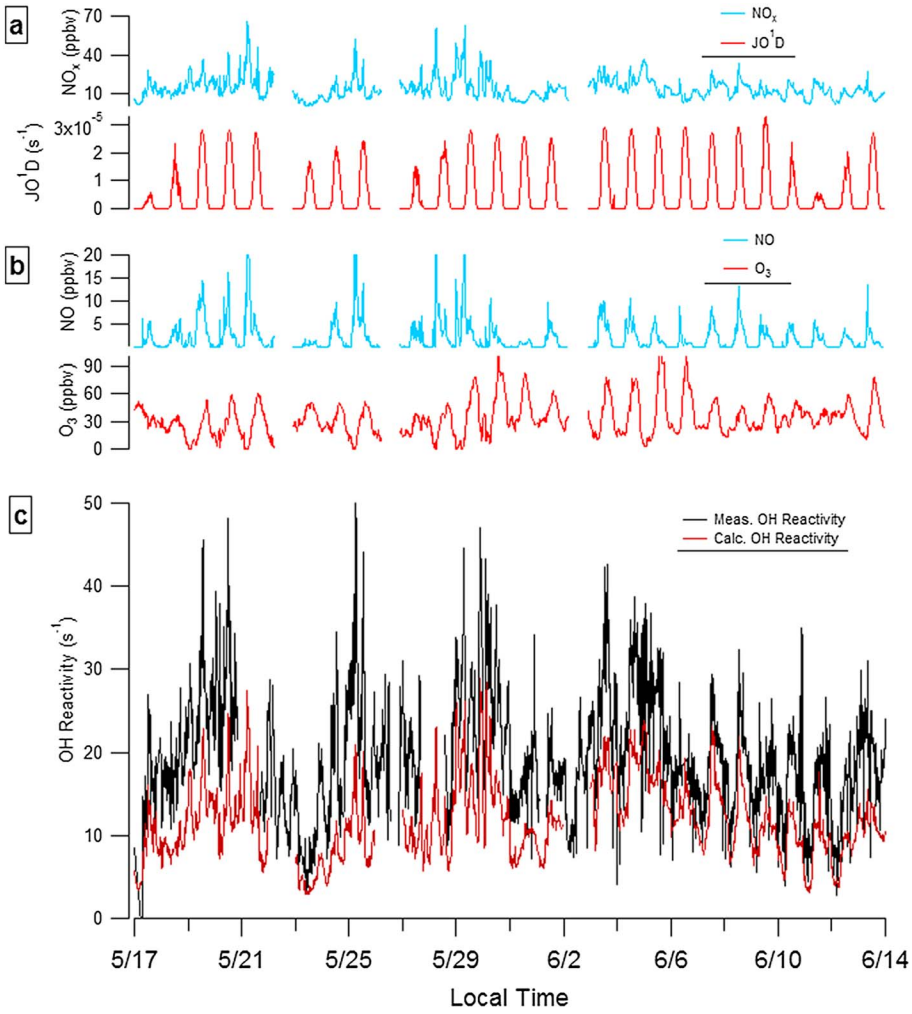

Figure 2. (a) Daily J(O^1D) and NO_x measurements and (b) daily ozone and nitric oxide measurements at the CalNex-LA site. (c) Measured (black) and RACM2 base model (red) OH reactivity. Times are PDT.

RO_2 detection efficiencies in the IU-FAGE instrument and the model predicted RO_2 concentrations, RO_2 radicals on average contributed 30 ± 10% to the modeled HO_2* concentrations, with peroxy radicals from isoprene and its oxidation products (ISOP, MACP, MVKP) accounting for approximately 50% and 40% of the modeled interference (αRO_2) on average for the weekends and weekdays, respectively, during the daytime (9 A.M. to 6 P.M.), with olefins (OLTP, OLIP) contributing approximately 20% (weekends) and 30% (weekdays) to the modeled interference during the daytime. Modeled HO_2* concentrations on the higher NO_x conditions observed on the weekdays generally underpredict the measurements, except for a few weekdays scattered throughout the early and later parts of the campaign. Better agreement is observed for the lower NO_x conditions of the weekends and holiday in contrast to that observed for OH.

Bivariate regressions (accounting for uncertainties in both the *x* and *y* directions) [*Deming*, 1943] of the daytime (6 A.M. to 9 P.M.) OH and HO_2* measurements with the RACM2 model predictions are shown in Figure 3. The data are separated between weekdays (Monday–Friday, except the holiday on 31 May) and the weekends + holiday during the campaign to reflect the average difference in NO_x observed on these days. The slopes of the OH regression plots indicate that RACM2 overpredicts OH concentrations by a factor of approximately 1.4 ± 0.3 (1σ) during the lower NO_x conditions on the weekend + holiday, while weekday OH concentrations are in good agreement with the models, with a slope of approximately 1.0 ± 0.2. In contrast to OH, the model underpredicts the measured HO_2* concentrations by a factor of approximately 3.0 ± 0.5 (1σ) during the high NO_x conditions during the week, while on the lower NO_x conditions on the weekends, measured HO_2* is only underpredicted

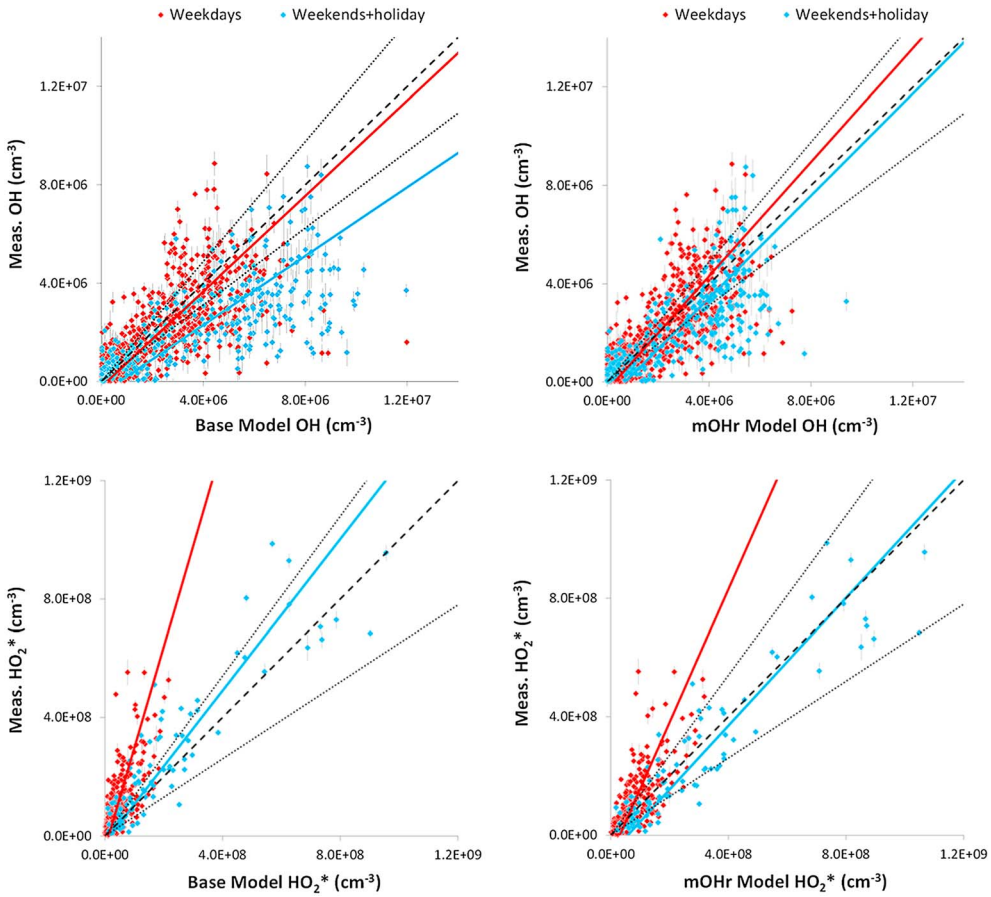

Figure 3. OH and HO_2* bivariate regressions of measured HO_x versus RACM2 (left) base and (right) mOHr HO_x, accounting for the 1σ model and measurement uncertainties. Each plot is split between the weekday data in red (M-F, except holiday) and weekends + holiday in blue. A 1:1 correlation is shown as the dashed line, and the 1σ modeling uncertainty is shown as the dotted lines.

by a factor of approximately 1.3 ± 0.2 (Figure 3). Because NO_x is constrained to the measured concentrations, this difference in the model agreement between the weekends and the weekdays is not the result of inaccuracies in the simulation of NO_x in the RACM2 box model but could suggest that important radical processes are missing from the model.

Measured nighttime (11 P.M. to 4 A.M.) OH concentrations at the CalNex-LA site were below the IU-FAGE instrument's limit of detection (4.4×10^5 cm^{-3}) more than 90% of the time. The few measurements that were significantly above the detection limit were generally higher than the model predictions and scattered across a few nights, similar to that observed in other urban campaigns [*Stone et al.,* 2012]. Reported nighttime OH radical concentrations in polluted environments have ranged from below 2×10^5 cm^{-3} [*Geyer et al.,* 2003] to above 1×10^6 cm^{-3} [*Lu et al.,* 2013]. The reason for the model underprediction of the few instances at night is unclear but could involve unknown measurement interferences that might not be accounted for using the C_3F_6 scavenging technique such as interferences from NO_3 radicals [*Fuchs et al.,* 2016]. Future work will involve tests to determine whether the IU-FAGE instrument is sensitive to interferences from NO_3 radicals at night and whether the concentrations of C_3F_6 added to scavenge OH also remove ambient NO_3. Other potential reasons for the model underprediction at night could involve an incomplete characterization of nighttime radical chemistry in the model or nocturnal transport of peroxy radicals followed by reaction with surface NO (see below). Measured nighttime HO_2* concentrations gradually decreased throughout the night, decreasing from approximately 8×10^7 cm^{-3} to 2×10^7 cm^{-3} between 11 P.M and 4 A.M. on average. These values are generally within the range of measured nighttime HO_2 concentrations reported for polluted environments [*Stone et al.,* 2012].

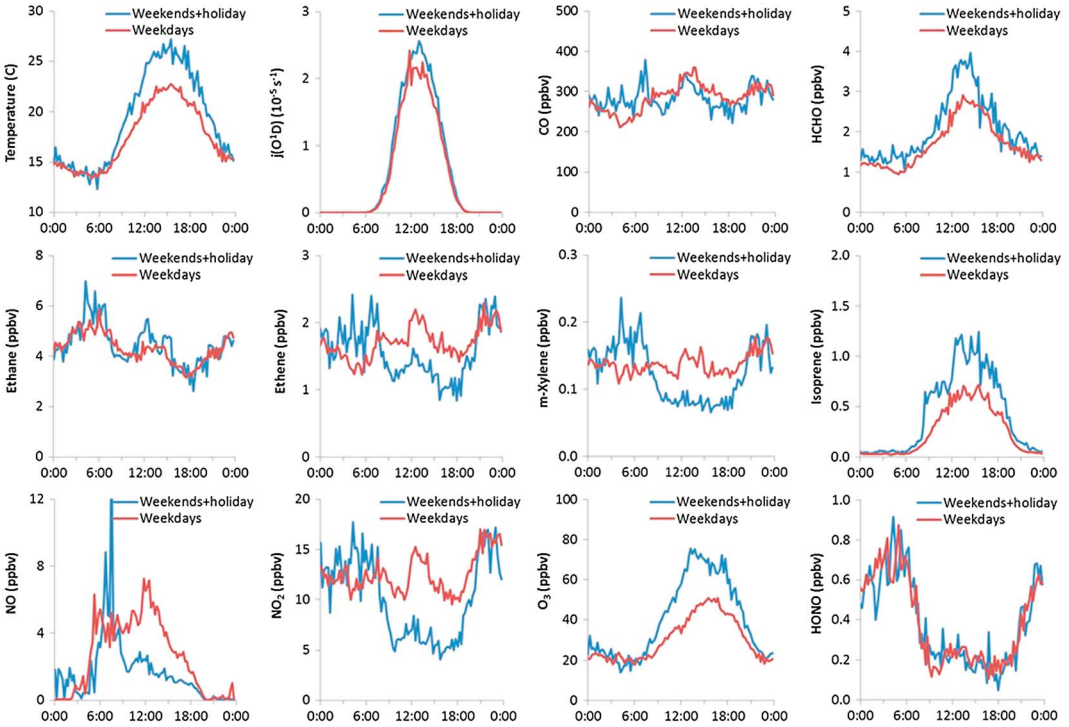

Figure 4. Diurnal average weekends + holiday ($N = 8$) (blue) and weekday ($N = 17$) (red) temperature, photolysis rates, and mixing ratios for key constraints used in the model. All times are local time (PDT).

3.2. Campaign Average OH and HO_2* Measurements and Model Results

Campaign diurnal average NO_x and VOC concentrations, temperature, and photolysis rates are shown in Figure 4. During the campaign, temperatures on the weekends and the Memorial Day holiday were on average 4°C warmer at peak afternoon hours than during the weekdays, contributing to the greater isoprene mixing ratios observed on the weekends + holiday. NO and NO_2 average mixing ratios were greater during the weekdays after 9 A.M. when the CalNex-LA site began to receive polluted air from elsewhere in the LA basin. Ozone mixing ratios have the opposite trend, where average ozone mixing ratios are approximately 20 ppbv greater on the weekends during the campaign. The trend of lower NO_x and higher ozone mixing ratios on the weekends has been observed before in the LA-basin [*Yarwood et al.*, 2003], and *Pollack et al.* [2012] also observed this trend for the CalNex campaign.

Weekday and weekends + holiday diurnal average measured values of OH and HO_2* are shown in Figure 5 with the average RACM2 modeled values (black line). The average peak concentrations of OH and HO_2* measured during CalNex-LA were similar to that observed in other urban areas (Table 1 and supporting information). The model is able to reasonably reproduce the observed diurnal OH concentration profile during the higher NO_x conditions during the week but overpredicts the observed OH on the lower NO_x conditions on the weekends + holiday by a factor of approximately 1.4 ± 0.3 (1σ) at midday. The overprediction of OH is outside of the 1σ combined uncertainty of the measurements and the model for the weekends + holiday comparison during the morning hours (8 A.M. to 12 P.M.). Although the model-measurement disagreement on the weekends is not significant at the 2σ level of uncertainty, it is unlikely that the calibration of the instrument varied systematically between the weekdays and the weekends. Given that the model agrees well with the measurements during the week, this suggests that the disagreement of the model with the measurements on the weekends is robust.

Average measured HO_2* concentrations show a distinct difference between the weekend and weekday profiles likely due to the differences in NO_x on these days, although differences in temperature and photolysis rates between the weekends and the weekdays could also contribute to the difference. Maximum HO_2* concentrations were a factor of 2 higher during the lower NO_x conditions on the weekends compared to the

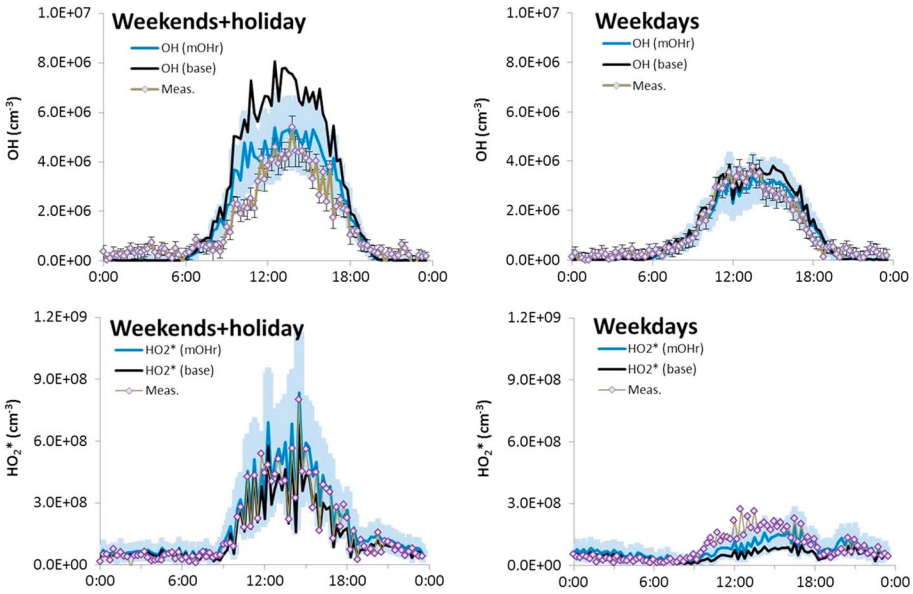

Figure 5. Diurnal average measurements of OH and HO_2* (markers) together with the base RACM2 model results (black) and the results from constraining the RACM2 model to the observed reactivity (mOHr, blue). Error bars reflect the 2σ precision of the measurement and are separate from the 2σ calibration accuracy of 36% for both OH and HO_2*. The size of the error bars for the HO_2* measurements are approximately the size of the data markers. Modeled 1σ uncertainties (shaded area) are 22.5% for OH and 35% for HO_2* and are only shown for the RACM2 results with the (mOHr) scenario. All times are local time (PDT).

higher NO_x conditions on weekdays. In contrast to the results for OH, RACM2 is able to reproduce the observed average weekends + holiday diurnal HO_2* profile reasonably well, while the model underpredicts the observed concentrations of HO_2* by a factor of approximately 3.0 ± 0.5 (1σ) at midday during the higher NO_x conditions during the week and is significant at the 2σ level of the combined uncertainty.

Campaign average measured nighttime OH concentrations, although greater than the model predictions, were generally near the campaign averaged detection limit of the instrument (1.0×10^5 cm^{-3}, campaign average 15 min interval LOD). Average nighttime HO_2* concentrations (approximately 3.0×10^7 cm^{-3}) were generally in good agreement with the model. The lifetime of peroxy radicals at night is variable depending on the NO mixing ratio but can reach up to 15 min. As a consequence, the assumption that transport of these radical species is negligible in and out of the modeled box can break down in some cases. Therefore, nocturnal transport of RO_2 followed by reaction of RO_2 with ground layer emissions of NO could form HO_2 and OH. *Geyer and Stutz* [2004] showed using a 1-D chemistry-transport model constrained for urban conditions that oxidation of VOCs in the upper part of the nocturnal boundary layer, for example, by the NO_3 radical, combined with vertical transport can cause distinctly enhanced levels of OH and HO_2 (up to 50% greater) throughout the 10 m layer near the surface.

4. Discussion

4.1. Analysis of the Model-Measurement Discrepancy

To gain insights into the measurement-model discrepancies, the base RACM2 model was modified to constrain the model to the total OH reactivity measurements (Figure 2) (Hansen et al., in preparation). Previous studies have shown that measurements of total OH reactivity in urban areas are sometimes significantly greater than that calculated from the measured concentrations of OH sinks [*Martinez et al.,* 2003; *Shirley et al.,* 2006; *Dolgorouky et al.,* 2012]. Figure 6 shows that the average measured total OH reactivity ($k_{OH,\ meas}$) at the CalNex-LA site on both the weekdays, and the weekends + holiday was consistently higher than modeled RACM2 OH reactivity (k_{OH_model}) by a factor of 1.7 on average. The modeled reactivity includes the reactivity from the measured VOCs and inorganics and the additional OH reactivity from secondary species (<10% of the total) calculated by the model during the 5 day spin-up. The average measured OH

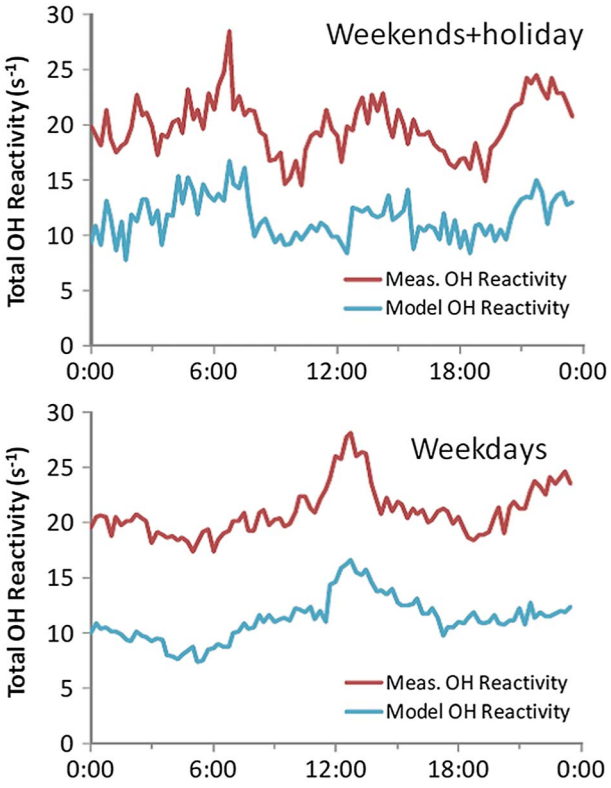

Figure 6. Average measured OH reactivity (red) and RACM2 modeled OH reactivity (blue) for the (top) weekends + holiday and (bottom) weekdays. All times are local time (PDT).

reactivity on the weekdays reached a maximum of approximately 28 s^{-1} at midday, while the measured OH reactivity on the weekends was similar in magnitude but did not exhibit a significant diurnal trend, with values typically between 18 and 22 s^{-1}. These values are approximately 7–10 s^{-1} greater than that calculated by the RACM2 model (Figure 6).

To constrain the RACM2 model to the observed OH reactivity, a multiplicative factor (>1) was introduced for lumped RACM2 surrogate species that were also constrained in the model. Based on the reactivity from these constrained VOCs, the multiplier was calculated at each time point to match the missing OH reactivity (supporting information). The resulting model-calculated OH reactivity was at some time points a few percent greater than the measured value due to the production of greater secondary oxidation species as a result of the increased OH reactivity.

Assuming that the missing reactivity consists of a mix of saturated hydrocarbons and aldehydes similar to that measured at the site ("mOHr" scenario), the agreement is improved for both OH and HO_2* (Figures 1 and 3) when the multiplier was increased for these species. Including an unmeasured unsaturated VOC species that reacts with ozone substantially increases the modeled nighttime HO_2* to unreasonable concentrations (2–4 × 10^8 cm^{-3}), which suggest that the missing OH reactivity, was not due to unsaturated VOCs. Assuming that the missing reactivity consists only of OVOCs as a mix of alcohols and aldehydes also improves the model agreement for both OH and HO_2*, although the model with this missing VOC mix still tends to overpredict the measured OH during the low NO_x conditions on the weekend + holiday (supporting information). Other compounds (e.g., ketones) had minimal impact in any scenario due to their low contribution to OH reactivity.

Figure 5 also compares the results of the mOHr increased reactivity scenario (blue line) with the diurnal average values of OH and HO_2*. For the higher NO_x conditions on the weekdays, adding the missing OH reactivity increases the modeled HO_2* by approximately 50–70% while resulting in relatively small decreases in the modeled OH concentrations, as decreases in the OH radical concentrations due to the increased reactivity appear to be well buffered by increased OH production from the $HO_2 + NO \rightarrow OH + NO_2$ reaction under the higher weekday NO conditions due to the increase in HO_2* concentrations in this scenario. For the lower NO_x conditions on the weekends + holiday, adding the missing OH reactivity reduces the modeled OH by approximately 25% while increasing the modeled HO_2* by less than 10%, as increases in the HO_2* concentrations appear to be buffered by increases in the rate of loss of HO_2* by the $RO_2 + HO_2$ reaction under the lower weekend NO conditions. The resulting calculated OH concentrations on the lower NO_x conditions on the weekends + holiday are in better agreement with the observations, while modeled HO_2* concentrations are still in good agreement with the measurements (Figures 3 and 5). The discrepancy between the measured and modeled OH generally increases with decreasing mixing ratios of NO_x, with the greatest model overestimation occurring under conditions when NO_x was less than 5 ppb (supporting information).

For the higher NO_x conditions on the weekdays, adding the missing OH reactivity in the model does not impact the agreement with that observed for OH but improves the agreement for HO_2* (Figures 3 and 5).

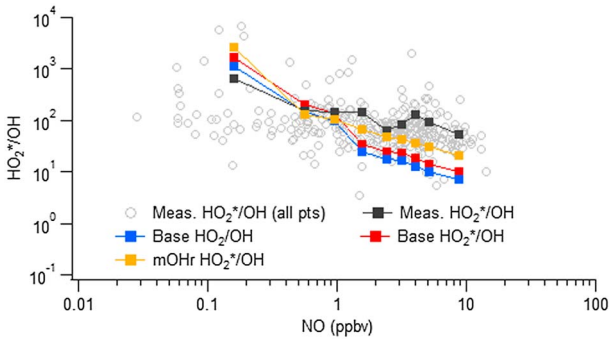

Figure 7. Individual measured (open circles) and average measured (black squares) HO_2*/OH versus NO (6 A.M. to 9 P.M.) with the average base RACM2 model results (red squares) and the mOHr model results (gold squares). The RACM2 base-modeled HO_2/OH ratio (blue squares) is shown for comparison.

However, the model still underpredicts the observed HO_2* concentrations on the weekdays by a factor 2 ± 1 (1σ) on average. The discrepancy between the measured and modeled HO_2* increases with increasing mixing ratios of NO_x, with the greatest model underestimation occurring under conditions when NO_x was greater than approximately 15 ppb (supporting information). To bring the modeled HO_2* into agreement with the measurements would require an OH reactivity 25% greater than measured. This discrepancy could reflect an underestimation of the contribution of RO_2 radicals to the measurement of HO_2* under these conditions, although it is unlikely that uncertainties associated with the RO_2 interference alone could explain the difference.

Peroxyacetyl nitrate (PAN) and other acyl peroxynitrates can be long-lived species relative to the radical lifetime that can impact both the concentrations of RO_x and NO_x. An incomplete characterization of this chemistry could impact the modeled radical concentrations. Both the base and mOHr models were tested by unconstraining the PAN concentration to compare model predicted concentrations to measurements while ignoring transport but including dry deposition (see supporting information). The base RACM2 model underpredicts the measured PAN concentrations by up to a factor of 2 on average throughout the daytime during the weekdays and weekends + holiday. However, after applying the mOHr scenario to account for the measured missing OH reactivity, the measured and modeled PAN concentrations were in agreement to within 30%, which is within the combined uncertainty of the model and the measurements, giving confidence in the model's treatment of this chemistry.

The ratio of HO_2/OH has often been used as a metric to test our understanding of the cycling chemistry between RO_x radicals [*Ren et al.,* 2003a, 2003b; *Martinez et al.,* 2003; *Emmerson et al.,* 2005; *Shirley et al.,* 2006; *Dusanter et al.,* 2009a, 2009b; *Sheehy et al.,* 2010]. Because of the RO_2 interference associated with the HO_2 measurements, the HO_2*/OH ratio is presented here. Figure 7 displays the measured and modeled HO_2*/OH ratio as a function of NO in addition to the modeled HO_2/OH ratio, illustrating that the HO_2*/OH ratio responds to changes in NO similar to the HO_2/OH ratio. The observed ratio varies from an average value of approximately 100 at NO mixing ratios less than 1 ppbv to an average value of approximately 40 at 10 ppbv of NO. These ratios are generally greater than the base model predictions, although the agreement is better at NO mixing ratios around 1 ppbv. Similar results have been observed in previous campaigns comparing measured and modeled HO_2/OH ratios [*Ren et al.,* 2003a, 2003b; *Martinez et al.,* 2003; *Emmerson et al.,* 2005; *Dusanter et al.,* 2009b]. It must be noted that the HO_2 measurements performed during these studies could have been impacted by potential interferences from RO_2 radicals. For the measurements reported here, comparing the modeled HO_2*/OH ratio instead of the modeled HO_2/OH ratio to the measured ratio improves the agreement, but the model still underestimates the measurements at higher NO mixing ratios (Figure 7). However, constraining the RACM2 model to the observed total OH reactivity increases the modeled ratio and brings it into better agreement with the measurements, although the model still appears to underestimate the measurements during the high NO weekday periods (Figure 7).

4.2. Radical Budget Analysis

A rate of production analysis can provide information about the key processes driving RO_x production and loss. RO_x production and loss are divided into initiation, termination, and propagation pathways to more specifically describe the sources and sinks of OH, HO_2, RO_2, and total RO_x. RO_x radical initiation routes are defined as those leading to new RO_x radical formation, with primary contributions from photolysis routes and ozone-alkene reactions. Termination routes are chemical reactions removing RO_x radicals from the system with

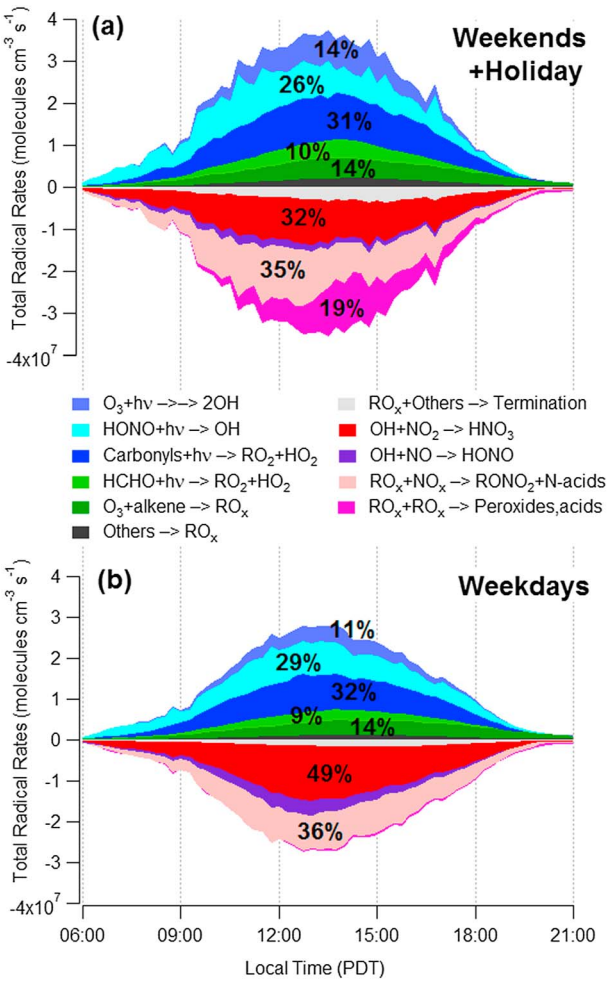

Figure 8. Total RO_x radical budgets from the mOHr RACM2 model including the sources and sinks for OH, HO_2, and RO_2 radicals for the average (a) weekends + holiday and (b) weekdays. All times are local time (PDT).

either cross and self-reactions of radicals or reactions involving NO_x species, the extent of each depending on the mixing ratio of NO_x. Finally, propagation routes convert one RO_x radical into another (e.g., $HO_2 + NO \rightarrow OH + NO_2$). Thus, propagation routes are a component of both overall production and loss for the individual OH, HO_2, and RO_2 radicals, while initiation and termination routes relate only to total radical production and loss, respectively.

Figures 8 and 9 show the daytime radical budget based on the results of the RACM2 model constrained by the measured total reactivity (RACM2 mOHr) with the results averaged for weekends + holiday and weekdays during the campaign. Figure 8 illustrates the total radical initiation and termination budget as a function of time of day for the weekends + holiday and the weekends, while Figure 9 illustrates the daily average rates of radical initiation, propagation, and termination for the weekends + holiday (blue) and weekdays (red). As illustrated in these figures, the overall magnitude of RO_x ($OH + HO_2 + RO_2$), radical initiation, and termination was approximately 1.3 times greater on the weekends compared to the weekdays, primarily due to higher *J* values and radical precursor concentrations (HCHO, O_3) on weekends (Figure 4). HONO photolysis was an important radical initiation route on both weekends and weekdays, accounting for 26–30% of the total daily radical initiation rate on average at this height. HONO photolysis accounts for approximately 60% of total radical initiation and 20% of OH gross production in the early morning before 10 A.M. (average diurnal profiles of the individual OH, HO_2, and RO_2 radical budgets are illustrated in the supporting information). It is interesting to note that unconstraining the HONO concentration in the model leads to model-predicted HONO concentrations that are approximately 1.3 times lower than the measurements and significantly underpredicts the observed concentrations of both OH and HO_2* radicals, suggesting that although the gas phase production of HONO from the OH + NO reaction in the model can explain approximately 70–80% of the observed HONO on average, there is a significant source of HONO missing from the model at this measurement height (see supporting information).

The contribution of HONO to total radical initiation during CalNex-LA was similar to that observed in several previous field campaigns where HONO concentrations were measured directly and used to constrain the model. In these studies, the calculated contributions of HONO photolysis to total radical initiation were generally greater than 20% (Table S1 in the supporting information). In contrast, campaigns where HONO was not measured resulted in predicted contributions of HONO photolysis that were less than 10%. These results suggest that measurements of HONO are important in order to accurately reflect the contribution of HONO to radical initiation. However, it is important to note that this contribution of HONO photolysis to HO_x radical production is primarily relevant at the 10 m sampling height at the CalNex-LA site. Strong vertical gradients

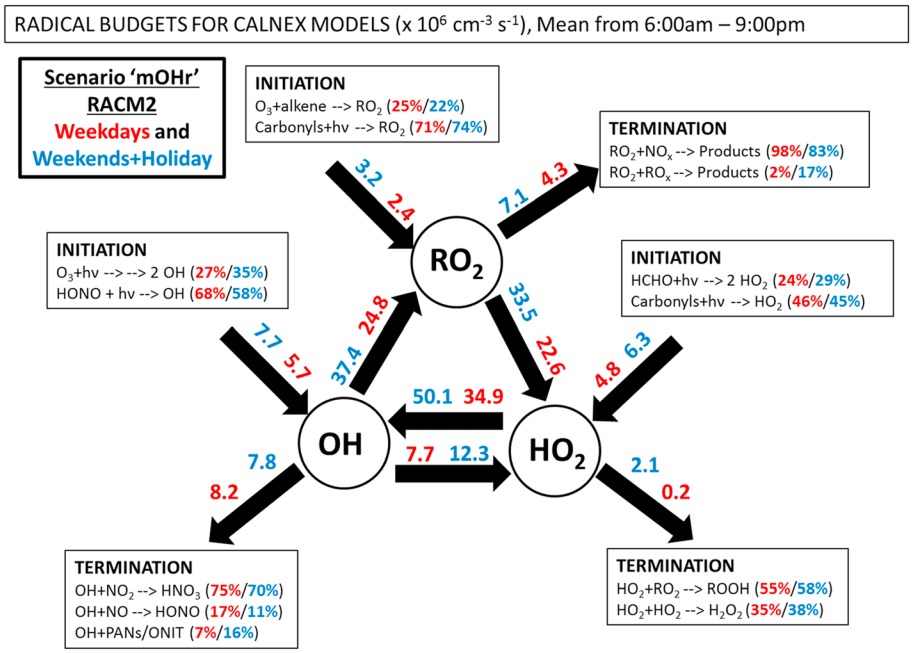

Figure 9. RO_x radical budget from the mOHr model scenario illustrating the average daytime (6 A.M. to 9 P.M.) radical initiation, propagation, and termination rates (in 10^6 cm^{-3} s^{-1}). Individual rates for the weekends + holiday are shown in blue, and weekday rates are shown in red.

of HONO were observed at this site [*Young et al.,* 2012], and thus, the contribution of HONO to HO_x production described in this analysis should be considered an upper limit for the contribution of HONO to HO_x radical production integrated across the boundary layer.

Photolysis of formaldehyde and other carbonyls together accounted for approximately 40% of total radical initiation, while the contribution of ozone photolysis and alkene ozonolysis was less than 15% on both weekdays and weekends + holiday. The contribution of formaldehyde and other OVOC photolysis during CalNex-LA was similar to that observed in other urban campaigns, contributing to between 30 and 60% of total radical initiation (Table S1). The contributions of alkene ozonolysis and ozone photolysis to total radical production during CalNex-LA of less than 15% were similar to that observed in many of the more recent urban campaigns where comprehensive measurements of VOCs and in particular alkenes were made, also illustrating the importance of these measurements to understanding the radical budget. The contribution of $ClNO_2$ photolysis to radical production was not considered in this analysis. However, *Young et al.* [2012] showed that radical production from $ClNO_2$ photolysis was similar to that from HONO photolysis at the surface in the early morning and potentially becoming more important when integrated across the entire boundary layer.

Important propagation routes for the OH and HO_2 budgets are shown in comparison to OH and HO_2 initiation and termination routes in Figure S8. Due to fast nitrogen oxide chemistry, even on the weekends with lower NO_x, the propagation routes of OH to RO_2, OH to HO_2, RO_2 to HO_2, and HO_2 to OH dominate and account for more than 80% of the total production and loss of both OH and HO_2. The OH + NO_2 reaction leading to the formation of nitric acid (HNO_3) was the dominant RO_x radical termination route during the week (approximately 50% on average) while accounting for only 30% of total RO_x radical termination during the weekends + holiday (Figures 8 and 9). The formation of organic nitrates contributed to approximately 30% of radical termination on both weekdays and weekends, while radical termination from RO_x cross and self-reactions leading to the production of acids and peroxides contributed to less than 5% of the radical termination on average during the weekdays. However, on the weekends + holiday, radical termination by RO_x cross and self-reactions contributed to 20% of total radical termination on average during the day and contributed to approximately 50% of radical termination during the early afternoon (see supporting information).

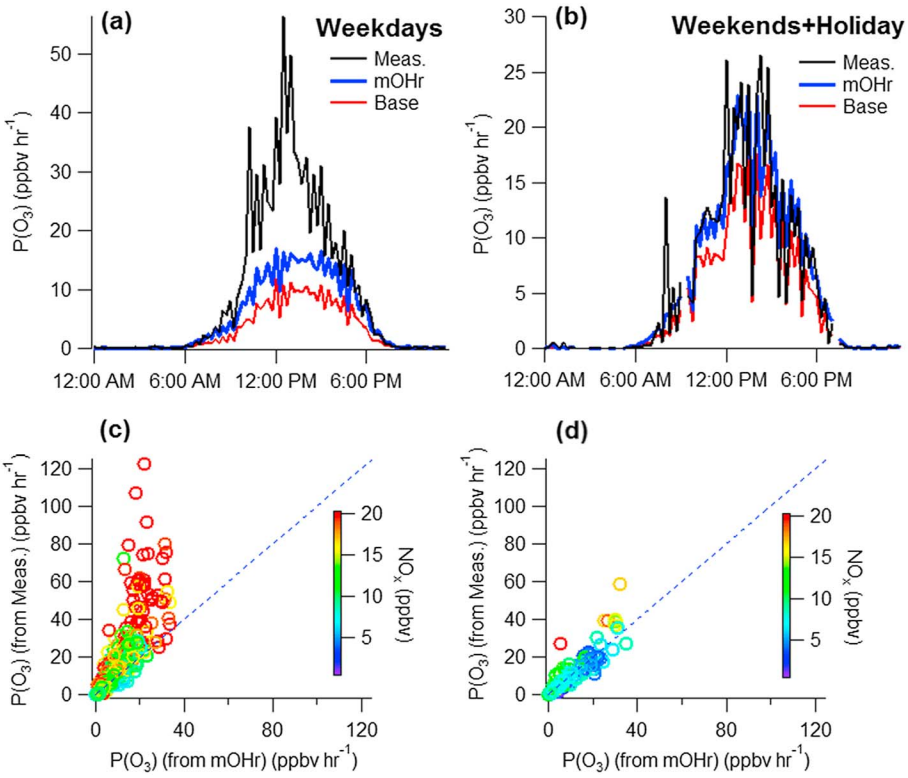

Figure 10. Diurnal average instantaneous rates of ozone production ($P(O_3)$) from the measurements and the base and mOHr models for the (a) weekdays and the (b) weekends. The correlation between the measured and mOHr modeled $P(O_3)$ as a function of NO_x for the (c) weekdays and the (d) weekend + holiday. All times are local time (PDT).

4.3. Rates of Instantaneous Ozone Production

The intantaneous rate of ozone production is driven by radical propagation and is also a good indicator of the cycling between OH and peroxy radicals. The gross rate of instantaneous ozone production ($P(O_3)$) can be expressed as the rate of NO_2 production by peroxy radicals [*Shirley et al.,* 2006]:

$$P(O_3) = k_{HO2+NO}[HO_2][NO] + \sum k_{RO2+NO}\phi_{RO2+NO}[RO_2][NO] \quad (2)$$

In this equation, ϕ_{RO2+NO} represents the yield of $RO + NO_2$ from the $RO_2 + NO$ reaction. Figure 10 shows the average $P(O_3)$ for both the higher NO_x conditions on the weekdays and the lower NO_x conditions on the weekends determined using the first term in equation (2) with measurements of OH, HO_2*, and NO_x. Note that using only the HO_2* measurements in this equation does not include ozone production from RO_2 radicals that were not detected by the IU-FAGE instrument.

As illustrated in Figure 10, the average $P(O_3)$ from HO_2* during the week reached a maximum of approximately 40–50 ppb h^{-1} near local noon, somewhat earlier than the observed peak in the diurnally averaged measured ozone (Figure 4), similar to that observed in other urban areas [*Ren et al.,* 2003a, 2003b; *Dusanter et al.,* 2009a; *Sheehy et al.,* 2010]. However, while surface ozone concentrations and instantaneous ozone production are strongly linked together, they are each characterized by different temporal and spatial scales. Measured ozone concentrations reflect an integration of $P(O_3)$ over a large spatial scale and a long time scale, while the calculations of instantaneous ozone production presented here do not take these issues into account. The measured instantaneous $P(O_3)$ during the weekends + holiday are on average lower than that observed during the week, with maximum values of approximately 25 ppb h^{-1} near local noon. Figure 10 also shows the calculated instantaneous $P(O_3)$ from the modeled HO_2* for the model constrained to the observed OH reactivity (mOHr), illustrating the underestimation of the measured $P(O_3)$ by the model on the weekdays due primarily to the underestimation of the measured HO_2* during the higher NO_x conditions during the week (Figure 5). Better

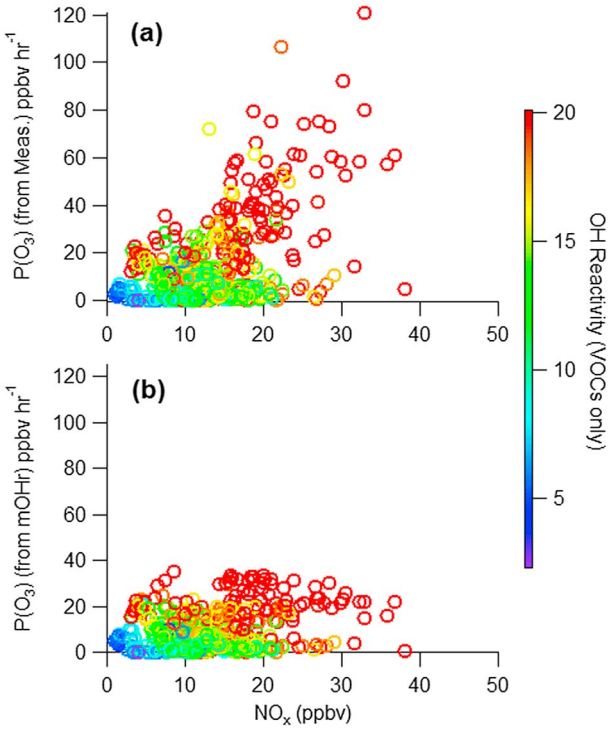

Figure 11. Instantaneous rates of ozone production (PO_3) as a function of NO_x and the OH reactivity from VOCs (s^{-1}) from the (a) measurements and the (b) mOHr model.

agreement between the modeled and measured HO_2* during the lower NO_x conditions on the weekends + holiday results in the model being able to reproduce the observed $P(O_3)$ during these days.

The correlation between the observed instantaneous $P(O_3)$ and the instantaneous $P(O_3)$ from the mOHr model as a function of NO_x for both the weekdays and the weekends + holiday is also illustrated in Figure 10. In general, the instantaneous $P(O_3)$ measured during the week was similar to that observed on the weekends except for weekday periods when NO_x was greater than approximately 15 ppb. During these times, the measured instantaneous $P(O_3)$ was greater than 40 ppb h^{-1} and sometimes greater than 100 ppb h^{-1}. The model is able to reproduce the observed $P(O_3)$ under the low NO_x conditions during the weekends but tends to underestimate the observed $P(O_3)$ during the week when NO_x concentrations were greater than approximately 10–15 ppb due to the model underestimation of the observed HO_2* concentrations under these conditions.

Figure 11 further illustrates the NO_x dependence of the measured and modeled instantaneous $P(O_3)$ for all days as a function of the OH reactivity due to VOCs. As can be seen from this figure, the model is generally able to reproduce the observed increase in ozone production with both NO_x and VOC reactivity for NO_x mixing ratios less than15 ppb, and the decrease in $P(O_3)$ with increasing NO_x for VOC reactivity less than 15 s^{-1}. However, the model tends to underpredict the measured $P(O_3)$ for NO_x mixing ratios greater than 15 ppb and VOC reactivity greater than 15 s^{-1}. This is consistent with the model underestimation of HO_2* and the HO_2*/OH ratio under these conditions and could reflect an underestimation of the contribution of RO_2 radicals to the measurement of HO_2* under these conditions, although it is unlikely that uncertainties associated with the RO_2 interference alone could explain the difference. The model underestimation of $P(O_3)$ together with the good agreement of the model with the OH measurements under high NO_x and high VOC reactivity could suggest that the radical propagation chemistry is not well understood under these conditions, perhaps due to the simplified peroxy radical chemistry in the RACM2 model or could also be indicative of segregation of peroxy radicals and NO in these air masses [*Kanaya et al.*, 2007]. Similar results have been observed in other urban areas [*Ren et al.,* 2003b; *Sheehy et al.,* 2010]. Future work will examine the ability of the explicit Master Chemical Mechanism model to reproduce the observed HO_2* concentration and rate of ozone production during the CalNex-LA campaign as well as a more detailed analysis of the discrepancy between the measured and modeled rates of ozone production.

4.4. Ozone Production Sensitivity

Kleinman et al. [1997, 2001] proposed a simple metric (L_N/Q) to determine the sensitivity of ozone production to changes in VOCs and NO_x. L_N is the rate of irreversible termination of RO_x radicals by reaction with NO_x (i.e., $OH + NO_2 \rightarrow HNO_3$, $OH + NO \rightarrow HONO$, $RO_2 + NO \rightarrow$ organic nitrates), while Q is the rate of total radical initiation. Using this metric, *Kleinman et al.* [1997] illustrated that L_N/Q values above 0.5 indicate that ozone production is VOC limited, while values below 0.5 suggest that ozone production is NO_x limited. The L_N/Q

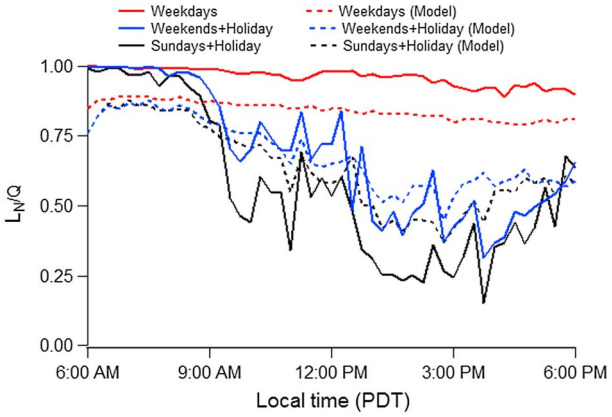

Figure 12. Average diurnal L_N/Q values calculated using the analytical equation from *Kleinman et al.* [2001] (solid lines) and calculated directly from the RACM2 mOHr modeled radical loss from NO_x (L_N) and total radical production (Q) (dashed lines). Weekday values (red) are compared to the weekends + holiday (blue) and Sundays + holiday (black). All times are local time (PDT).

ratio has been used to examine the sensitivity of ozone production in various urban areas [*Mao et al.,* 2010; *Edwards et al.,* 2013]. Measurements from New York City result in L_N/Q values close to 1.0 all day, suggesting that ozone production is VOC limited, but other urban areas such as Houston and Mexico City exhibit L_N/Q values that are greater than 0.5 in the morning but decreases to less than 0.5 in the afternoon, suggesting that ozone production sensitivity shifts from VOC limited to NO_x limited during the course of the day [*Mao et al.,* 2010].

Because all of the components of L_N/Q are not usually supported by measurements, *Kleinman et al.* [2001] developed an analytical expression that utilizes a smaller subset of measurements, including measurements of NO_x and total OH reactivity (supporting information). The total rate of radical initiation including O_3 photolysis, HONO photolysis, OVOC photolysis, and O_3-olefin reactions, incorporated measurements of O_3, H_2O, HONO, HCHO, C2–C4 straight chain aldehydes, methacrolein, glyoxal, and photolysis rate constants $J(O^1D)$, J(HONO), J(HCHO), and $J(CH_3CHO)$ for the calculation of radical initiation from the photolysis of ozone (followed by $O(^1D) + H_2O \rightarrow 2\ OH$), HONO, HCHO, CHOCHO, and other carbonyls. The ratio of $HO_2/(HO_2 + RO_2)$ was assumed to be 0.5, similar to that predicted by the RACM2 model. To account for other unmeasured photolytic radical sources, such as the photolysis of methylglyoxal and other dicarbonyls, model-estimated concentrations of these compounds were also incorporated into the Q value representing 10–15% of total radical initiation.

Diurnal average values of L_N/Q calculated from both the analytical expression and from the RACM2 model outputs of radical loss from NO_x (L_N) and total radical production (Q) for the weekdays and the weekends + holiday during the campaign are shown in Figure 12. Both the analytical expression and the RACM2 modeled L_N/Q exhibit similar trends, although the values calculated by the analytical expression are generally lower than the values determined from the model outputs. As illustrated in this figure, the L_N/Q trends suggest that ozone production was VOC limited during the weekdays and during the weekend mornings, as both the analytical expression and the direct model calculation of L_N/Q are greater than 0.5. However, during the afternoon on the weekends + holiday both the analytical expression and the model-calculated L_N/Q are both less than 0.5, suggesting that ozone production was NO_x limited. Including only Sundays and the Memorial Day holiday in the calculation results in even lower L_N/Q values in the afternoon. This weekend effect was due to lower concentrations of NO_x observed during the weekend afternoons compared to the weekdays, reducing the rate of radical termination by NO_x. These results suggest that continued NO_x reductions are likely to be increasingly effective at reducing weekend O_3, consistent with the recent observation of a weakening of the weekend ozone effect over this area [*Baidar et al.*, 2015]. A more detailed analysis of ozone production during the campaign, including the local role of isoprene will be presented in a subsequent paper.

5. Summary

The CalNex-LA campaign provided an opportunity to investigate RO_x radical chemistry in the Los Angeles, CA, basin. Measurements of OH and HO_2* radical concentrations during CalNex-LA exhibited a distinct weekend effect, with higher radical concentrations on the weekends due to lower NO_x levels. The RACM2 mechanism, constrained by measurements of long-lived trace gases, is generally able to reproduce the observed OH radical concentrations during the week when mixing ratios of NO were generally greater than 4 ppbv. However, the model does tend to overpredict the concentration of OH measured during the weekends + holiday by a factor of 1.4 ± 0.3 (1σ) when mixing ratios of NO were generally below 4 ppbv.

In contrast, the measurements of HO_2* concentrations are in reasonable agreement with the model on the weekends but are underpredicted by more than a factor of 3 during the week. Some of these discrepancies are likely due to an incomplete characterization of reactive trace gases, as the model underestimates the measured total OH reactivity. Constraining the model to the measured OH reactivity improves the agreement with the measured weekends + holiday OH and weekdays HO_2* concentrations, demonstrating the importance of including potential missing OH reactivity in order to accurately predict radical concentrations and instantaneous rates of ozone production in this environment. However, while constraining the model to the observed total OH reactivity improves the agreement with the measurements, HO_2* concentrations measured during weekdays are still underpredicted by approximately a factor of 2 ± 0.5 leading to an underprediction of the measured HO_2*/OH ratio at higher mixing ratios of NO, suggesting an incomplete understanding of the RO_x propagation chemistry. As a result of the underprediction of HO_2*, the model tends to underestimate the observed instantaneous rate of ozone production for NOx mixing ratios greater than 15 ppb and OH reactivity due to VOCs greater than $15\,s^{-1}$. The inability of the model to reproduce the observed $P(O_3)$ under these conditions could indicate that the radical propagation chemistry is not well understood under these conditions, perhaps due to the simplified peroxy radical chemistry in the RACM2 model or that there is significant segregation of peroxy radicals and NO in these air masses.

A radical budget analysis (6 A.M. to 9 P.M.) from the OH reactivity-constrained RACM2 model shows that HONO photolysis was an important radical initiation route on all days during the campaign, with an average daily contribution to the total initiation rate of RO_x radicals of approximately 26–30% (not including OH radical loss from HONO formation from the OH + NO reaction), although the contribution of HONO to radical production in the boundary layer is probably less given the observed vertical gradient in HONO concentrations at this site. Photolysis of formaldehyde and other carbonyls together accounted for approximately 40% of total radical initiation, while O_3 photolysis contributed less than 15% to the total initiation rate of radicals on average. Radical termination was dominated by the $OH + NO_2$ reaction during the week, but the lower NO_x and higher peroxy radical concentrations on the weekends resulted in a significant contribution of radical self and cross reactions to the overall radical termination rate (approximately 20% on average) but accounted for approximately 50% of total radical termination during the weekend afternoons. An analysis of the sensitivity of ozone production suggests that during the week ozone production was VOC limited throughout the day at the CalNex-LA site, while ozone production was NO_x limited during the afternoon on the weekends. Future work will involve a more detailed analysis of ozone production observed during the campaign in comparison to other urban areas.

Acknowledgments

This work was supported by grants from the National Science Foundation (AGS-0612738 and AGS-1104880). We would also like to thank the California Air Resources Board and the California Institute of Technology for their support of the CalNex-LA ground site. We would also like to thank Jean François Doussin and Marie Camredon from LISA for their valuable discussion. Data presented in this manuscript can be requested by contacting the corresponding author and can also be found at http://www.esrl.noaa.gov/csd/projects/calnex/.

References

Baidar, S., R. M. Hardesty, S.-W. Kim, A. O. Langford, H. Oetjen, C. J. Senff, M. Trainer, and R. Volkamer (2015), Weakening of the weekend ozone effect over California's South Coast Air Basin, *Geophys. Res. Lett.*, *42*, 9457–9464, doi:10.1002/2015GL066419.

Brasseur, G. P., D. A. Hauglustaine, S. Walters, P. J. Rasch, J. F. Muller, C. Granier, and X. X. Tie (1998), MOZART, a global chemical transport model for ozone and related chemical tracers 1. Model description, *J. Geophys. Res.*, *103*, 28,265–28,289, doi:10.1029/98JD02397.

Cantrell, C. A., J. G. Calvert, A. Bais, R. E. Shetter, B. L. Lefer, and G. D. Edwards (2003), Overview and conclusions of the International Photolysis Frequency Measurement and Modeling Intercomparison (IPMMI) study, *J. Geophys. Res.*, *108*(D16), 8542, doi:10.1029/2002JD002962.

Carslaw, N., P. J. Jacobs, and M. J. Pilling (1999), Modeling OH, HO2, and RO2 radicals in the marine boundary layer: 2. Mechanism reduction and uncertainty analysis, *J. Geophys. Res.*, *104*(D23), 30,257–30,273, doi:10.1029/1999JD900782.

Carslaw, N., et al. (2001), OH and HO2 radical chemistry in a forested region of north-western Greece, *Atmos. Environ.*, *35*, 4725–4737.

Chen, S. A., X. R. Ren, J. Q. Mao, Z. Chen, W. H. Brune, B. Lefer, B. Rappenglück, J. Flynn, J. Olson, and J. H. Crawford (2010), A comparison of chemical mechanisms based on TRAMP-2006 field data, *Atmos. Environ.*, *44*, 4116–4125, doi:10.1016/j.atmosenv.2009.05.027.

Czader, B. H., X. Li, and B. Rappenglueck (2013), CMAQ modeling and analysis of radicals, radical precursors, and chemical transformations, *J. Geophys. Res. Atmos.*, *118*, 11,376–11,387, doi:10.1002/jgrd.50807.

Deming, W. E. (1943), *Statistical Adjustment of Data*, Wiley, New York.

Derwent, R. G. (1996), The influence of human activities on the distribution of hydroxyl radicals in the troposphere, *Philos. Trans. R. Soc. A*, *354*, 501–531, doi:10.1098/rsta.1996.0018.

Di Carlo, P., et al. (2004), Missing OH reactivity in a forest: Evidence for unknown reactive biogenic VOCs, *Science*, *304*, 722–725, doi:10.1126/science.1094392.

Dlugi, R., et al. (2010), Turbulent exchange and segregation of HO_x radicals and volatile organic compounds above a deciduous forest, *Atmos. Chem. Phys.*, *10*, 6215–6235, doi:10.5194/acp-10-6215-2010.

Dolgorouky, C., V. Gros, R. Sarda-Esteve, V. Sinha, J. Williams, N. Marchand, S. Sauvage, L. Poulain, J. Sciare, and B. Bonsang (2012), Total OH reactivity measurements in Paris during the 2010 MEGAPOLI winter campaign, *Atmos. Chem. Phys.*, *12*, 9593–9612, doi:10.5194/acp-12-9593-2012.

Drummond, J. W., A. Volz, and D. H. Ehhalt (1985), An optimized chemiluminescence detector for tropospheric NO measurements, *J. Atmos. Chem.*, *2*, 287–306.

Dusanter, S., D. Vimal, and P. S. Stevens (2008), Technical note: Measuring tropospheric OH and HO_2 by laser-induced fluorescence at low pressure. A comparison of calibration techniques, *Atmos. Chem. Phys.*, *8*, 321–340.

Dusanter, S., D. Vimal, P. S. Stevens, R. Volkamer, and L. T. Molina (2009a), Measurements of OH and HO_2 concentrations during the MCMA-2006 field campaign—Part 1: Deployment of the Indiana University laser-induced fluorescence instrument, *Atmos. Chem. Phys.*, *9*, 1665–1685.

Dusanter, S., et al. (2009b), Measurements of OH and HO_2 concentrations during the MCMA-2006 field campaign—Part 2: Model comparison and radical budget, *Atmos. Chem. Phys.*, *9*, 6655–6675.

Edwards, P. M., et al. (2013), OH reactivity in a South East Asian tropical rainforest during the Oxidant and Particle Photochemical Processes (OP3) project, *Atmos. Chem. Phys.*, *13*, 9497–9514.

Emmerson, K. M., N. Carslaw, L. J. Carpenter, D. E. Heard, J. D. Lee, and M. J. Pilling (2005), Urban atmospheric chemistry during the PUMA campaign 1: Comparison of modelled OH and HO_2 concentrations with measurements, *J. Atmos. Chem.*, *52*, 143–164, doi:10.1007/s10874-005-1322-3.

Emmerson, K. M., et al. (2007), Free radical modelling studies during the UK TORCH Campaign in Summer 2003, *Atmos. Chem. Phys.*, *7*, 167–181.

Fuchs, H., B. Bohn, A. Hofzumahaus, F. Holland, K. D. Lu, S. Nehr, F. Rohrer, and A. Wahner (2011), Detection of HO_2 by laser-induced fluorescence: Calibration and interferences from RO_2 radicals, *Atmos. Meas. Tech.*, *4*, 1209–1225, doi:10.5194/amt-4-1209-2011.

Fuchs, H., et al. (2016), Investigation of potential interferences in the detection of atmospheric ROx radicals by laser-induced fluorescence under dark conditions, *Atmos. Meas. Tech.*, *9*, 1431–1447, doi:10.5194/amt-9-1431-2016.

George, L. A., T. M. Hard, and R. J. O'Brien (1999), Measurement of free radicals OH and HO_2 in Los Angeles smog, *J. Geophys. Res.*, *104*, 11,643–11,655, doi:10.1029/1998JD100113.

Gerbig, C., S. Schmitgen, D. Kley, A. Volz-Thomas, K. Dewey, and D. Haaks (1999), An improved fast-response vacuum-UV resonance fluorescence CO instrument, *J. Geophys. Res.*, *104*, 1699–1704, doi:10.1029/1998JD100031.

Geyer, A., and J. Stutz (2004), The vertical structure of OH-HO_2-RO_2 chemistry in the nocturnal boundary layer: A one-dimensional model study, *J. Geophys. Res.*, *109*, D16301, doi:10.1029/2003JD004425.

Geyer, A., et al. (2003), Nighttime formation of peroxy and hydroxyl radicals during the BERLIOZ campaign: Observations and modeling studies, *J. Geophys. Res.*, *108*(D4), 8249, doi:10.1029/2001JD000656.

Goldstein, A. H., and I. E. Galbally (2007), Known and unexplored organic constituents in the Earth's atmosphere, *Environ. Sci. Technol.*, *41*, 1514–1521.

Goliff, W. S., W. R. Stockwell, and C. V. Lawson (2013), The regional atmospheric chemistry mechanism, version 2, *Atmos. Environ.*, *68*, 174–185, doi:10.1016/j.atmosenv.2012.11.038.

Griffith, S. M., et al. (2013), OH and HO_2 radical chemistry during PROPHET 2008 and CABINEX 2009-part 1: Measurements and model comparison, *Atmos. Chem. Phys.*, *13*, 5403–5423, doi:10.5194/acp-13-5403-2013.

Haman, C. L., B. Lefer, and G. A. Morris (2012), Seasonal variability in the diurnal evolution of the boundary layer in a near-coastal urban environment, *J. Atmos. Oceanic Technol.*, *29*, 697–710, doi:10.1175/jtech-d-11-00114.1.

Hansen, R. F., et al. (2014), Measurements of total hydroxyl radical reactivity during CABINEX 2009—Part 1: Field measurements, *Atmos. Chem. Phys.*, *14*, 2923–2937.

Heard, D. E., and M. J. Pilling (2003), Measurement of OH and HO_2 in the troposphere, *Chem. Rev.*, *103*, 5163–5198.

Hofzumahaus, A., et al. (2009), Amplified trace gas removal in the troposphere, *Science*, *324*, 1702–1704.

Kanaya, Y., R. Q. Cao, H. Akimoto, M. Fukuda, Y. Komazaki, Y. Yokouchi, M. Koike, H. Tanimoto, N. Takegawa, and Y. Kondo (2007), Urban photochemistry in central Tokyo: 1. Observed and modeled OH and HO_2 radical concentrations during the winter and summer of 2004, *J. Geophys. Res.*, *112*, D21312, doi:10.1029/2007JD008670.

Kleinman, L. I., P. H. Daum, J. H. Lee, Y. N. Lee, L. J. Nunnermacker, S. R. Springston, L. Newman, J. WeinsteinLloyd, and S. Sillman (1997), Dependence of ozone production on NO and hydrocarbons in the troposphere, *Geophys. Res. Lett.*, *24*, 2299–2302, doi:10.1029/97GL02279.

Kleinman, L. I., P. H. Daum, Y. N. Lee, L. J. Nunnermacker, S. R. Springston, J. Weinstein-Lloyd, and J. Rudolph (2001), Sensitivity of ozone production rate to ozone precursors, *Geophys. Res. Lett.*, *28*, 2903–2906, doi:10.1029/2000GL012597.

Knote, C., et al. (2014), Simulation of semi-explicit mechanisms of SOA formation from glyoxal in aerosol in a 3-D model, *Atmos. Chem. Phys.*, *14*, 6213–6239, doi:10.5194/acp-14-6213-2014.

Konrad, S., et al. (2003), Hydrocarbon measurements at Pabstthum during the BERLIOZ campaign and modeling of free radicals, *J. Geophys. Res.*, *108*(D4), 8251, doi:10.1029/2001JD000866.

Kuster, W. C., B. T. Jobson, T. Karl, D. Riemer, E. Apel, P. D. Goldan, and F. C. Fehsenfeld (2004), Intercomparison of volatile organic carbon measurement techniques and data at La Porte during the TexAQS2000 Air Quality Study, *Environ. Sci. Technol.*, *38*, 221–228, doi:10.1021/es034710r.

Lefer, B., B. Rappenglück, J. Flynn, and C. Haman (2010), Photochemical and meteorological relationships during the Texas-II Radical and Aerosol Measurement Project (TRAMP), *Atmos. Environ.*, *44*, 4005–4013.

Lu, K. D., et al. (2012), Observation and modeling of OH and HO_2 concentrations in the Pearl River Delta 2006: A missing OH source in a VOC rich atmosphere, *Atmos. Chem. Phys.*, *12*, 1541–1569.

Lu, K. D., et al. (2013), Missing OH source in a suburban environment near Beijing: Observed and modeled OH and HO_2 concentrations in summer 2006, *Atmos. Chem. Phys.*, *13*, 1057–1080.

Luke, W. T. (1997), Evaluation of a commercial pulsed fluorescence detector for the measurement of low-level SO_2 concentrations during the Gas-Phase Sulfur Intercomparison Experiment, *J. Geophys. Res.*, *102*, 16,255–16,265, doi:10.1029/96JD03347.

Mao, J., et al. (2012), Insights into hydroxyl measurements and atmospheric oxidation in a California forest, *Atmos. Chem. Phys.*, *12*, 8009–8020, doi:10.5194/acp-12-8009-2012.

Mao, J. Q., et al. (2010), Atmospheric oxidation capacity in the summer of Houston 2006: Comparison with summer measurements in other metropolitan studies, *Atmos. Environ.*, *44*, 4107–4115, doi:10.1016/j.atmosenv.2009.01.013.

Martinez, M., et al. (2003), OH and HO_2 concentrations, sources, and loss rates during the Southern Oxidants Study in Nashville, Tennessee, summer 1999, *J. Geophys. Res.*, *108*(D19), 4617, doi:10.1029/2003JD003551.

Michoud, V., et al. (2012), Radical budget analysis in a suburban European site during the MEGAPOLI summer field campaign, *Atmos. Chem. Phys.*, *12*, 11,951–11,974, doi:10.5194/acp-12-11951-2012.

Mielke, L. H., A. Furgeson, and H. D. Osthoff (2011), Observation of $ClNO_2$ in a mid-continental urban environment, *Environ. Sci. Technol.*, *45*, 8889–8896, doi:10.1021/es201955u.

Mielke, L. H., et al. (2013), Heterogeneous formation of nitryl chloride and its role as a nocturnal NOx reservoir species during CalNex-LA 2010, *J. Geophys. Res. Atmos.*, *118*, 10,638–10,652, doi:10.1002/jgrd.50783.

Newman, S., et al. (2013), Diurnal tracking of anthropogenic CO_2 emissions in the Los Angeles basin mega-city during spring, 2010, *Atmos. Chem. Phys.*, *13*, 4359–4372, doi:10.5194/acp-13-4359-2013.
Novelli, A., K. Hens, C. Tatum Ernest, D. Kubistin, E. Regelin, T. Elste, C. Plass-Dülmer, M. Martinez, J. Lelieveld, and H. Harder (2014a), Characterisation of an inlet pre-injector laser-induced fluorescence instrument for the measurement of atmospheric hydroxyl radicals, *Atmos. Meas. Tech.*, *7*(10), 3413–3430.
Novelli, A., L. Vereecken, J. Lelieveld, and H. Harder (2014b), Direct observation of OH formation from stabilised Criegee intermediates, *Phys. Chem. Chem. Phys.*, *16*, 19,941–19,951.
Peeters, J., T. L. Nguyen, and L. Vereecken (2009), HO_x radical regeneration in the oxidation of isoprene, *Phys. Chem. Chem. Phys.*, *11*, 5935–5939.
Peeters, J., J.-F. Müller, T. Stavrakou, and V. S. Nguyen (2014), Hydroxyl radical recycling in isoprene oxidation driven by hydrogen bonding and hydrogen tunneling: The upgraded LIM1 mechanism, *J. Phys. Chem. A*, *118*(38), 8625–8643.
Pollack, I. B., B. M. Lerner, and T. B. Ryerson (2010), Evaluation of ultraviolet light-emitting diodes for detection of atmospheric NO2 by photolysis—Chemiluminescence, *J. Atmos. Chem.*, *65*, 111–125, doi:10.1007/s10874-011-9184-3.
Pollack, I. B., et al. (2012), Airborne and ground-based observations of a weekend effect in ozone, precursors, and oxidation products in the California South Coast Air Basin, *J. Geophys. Res.*, *117*, D00V05, doi:10.1029/2011JD016772.
Rappenglück, B., P. K. Dasgupta, M. Leuchner, Q. Li, and W. Luke (2010), Formaldehyde and its relation to CO, PAN, and SO_2 in the Houston-Galveston airshed, *Atmos. Chem. Phys.*, *10*, 2413–2424.
Ren, X., et al. (2008), HO_x chemistry during INTEX-A 2004: Observation, model calculation, and comparison with previous studies, *J. Geophys. Res.*, *113*, D05310, doi:10.1029/2007JD009166.
Ren, X., et al. (2012), Airborne intercomparison of HO_x measurements using laser-induced fluorescence and chemical ionization mass spectrometry during ARCTAS, *Atmos. Meas. Tech.*, *5*, 2025–2037, doi:10.5194/amt-5-2025-2012.
Ren, X., et al. (2013), Atmospheric oxidation chemistry and ozone production: Results from SHARP 2009 in Houston, Texas, *J. Geophys. Res. Atmos.*, *118*, 5770–5780, doi:10.1002/jgrd.50342.
Ren, X. R., H. Harder, M. Martinez, R. L. Lesher, A. Oliger, T. Shirley, J. Adams, J. B. Simpas, and W. H. Brune (2003a), HO_x concentrations and OH reactivity observations in New York City during PMTACS-NY2001, *Atmos. Environ.*, *37*, 3627–3637, doi:10.1016/s1352-2310(03)00460-6.
Ren, X. R., et al. (2003b), OH and HO_2 chemistry in the urban atmosphere of New York City, *Atmos. Environ.*, *37*, 3639–3651, doi:10.1016/s1352-2310(03)00459-x.
Ren, X. R., H. Harder, M. Martinez, I. C. Faloona, D. Tan, R. L. Lesher, P. Di Carlo, J. B. Simpas, and W. H. Brune (2004), Interference testing for atmospheric HO_x measurements by laser-induced fluorescence, *J. Atmos. Chem.*, *47*, 169–190, doi:10.1023/b:joch.0000021037.46866.81.
Roberts, J. M., et al. (2010), Measurement of HONO, HNCO, and other inorganic acids by negative-ion proton-transfer chemical-ionization mass spectrometry (NI-PT-CIMS): Application to biomass burning emissions, *Atmos. Meas. Tech.*, *3*, 981–990, doi:10.5194/amt-3-981-2010.
Rohrer, F., and H. Berresheim (2006), Strong correlation between levels of tropospheric hydroxyl radicals and solar ultraviolet radiation, *Nature*, *442*(7099), 184–187.
Rohrer, F., et al. (2014), Maximum efficiency in the hydroxyl-radical-based self-cleansing of the troposphere, *Nat. Geosci.*, *7*, 559–563.
Ryerson, T. B., et al. (2013), The 2010 California Research at the Nexus of Air Quality and Climate Change (CalNex) field study, *J. Geophys. Res. Atmos.*, *118*, 5830–5866, doi:10.1002/jgrd.50331.
Sheehy, P. M., R. Volkamer, L. T. Molina, and M. J. Molina (2010), Oxidative capacity of the Mexico City atmosphere—Part 2: A RO_x radical cycling perspective, *Atmos. Chem. Phys.*, *10*, 6993–7008.
Shetter, R. E., and M. Muller (1999), Photolysis frequency measurements using actinic flux spectroradiometry during the PEM-Tropics mission: Instrumentation description and some results, *J. Geophys. Res.*, *104*, 5647–5661, doi:10.1029/98JD01381.
Shirley, T. R., et al. (2006), Atmospheric oxidation in the Mexico City Metropolitan Area (MCMA) during April 2003, *Atmos. Chem. Phys.*, *6*, 2753–2765.
Stone, D., L. K. Whalley, and D. E. Heard (2012), Tropospheric OH and HO_2 radicals: Field measurements and model comparisons, *Chem. Soc. Rev.*, *41*, 6348–6404, doi:10.1039/c2cs35140d.
Thalman, R., and R. Volkamer (2010), Inherent calibration of a blue LED-CE-DOAS instrument to measure iodine oxide, glyoxal, methyl glyoxal, nitrogen dioxide, water vapour and aerosol extinction in open cavity mode, *Atmos. Meas. Tech.*, *3*, 1797–1814, doi:10.5194/amt-3-1797-2010.
Veres, P., J. M. Roberts, C. Warneke, D. Welsh-Bon, M. Zahniser, S. Herndon, R. Fall, and J. de Gouw (2008), Development of negative-ion proton-transfer chemical-ionization mass spectrometry (NI-PT-CIMS) for the measurement of gas-phase organic acids in the atmosphere, *Int. J. Mass Spectrom.*, *274*, 48–55, doi:10.1016/j.ijms.2008.04.032.
Veres, P. R., et al. (2011), Evidence of rapid production of organic acids in an urban air mass, *Geophys. Res. Lett.*, *38*, L17807, doi:10.1029/2011GL048420.
Volkamer, R., P. Sheehy, L. T. Molina, and M. J. Molina (2010), Oxidative capacity of the Mexico City atmosphere—Part 1: A radical source perspective, *Atmos. Chem. Phys.*, *10*, 6969–6991.
Warneke, C., et al. (2011), Airborne formaldehyde measurements using PTR-MS: Calibration, humidity dependence, inter-comparison and initial results, *Atmos. Meas. Tech.*, *4*, 2345–2358, doi:10.5194/amt-4-2345-2011.
Warneke, C., et al. (2013), Photochemical aging of volatile organic compounds in the Los Angeles Basin: Weekend effect, *J. Geophys. Res. Atmos.*, *118*, 5018–5028, doi:10.1002/jgrd.50423.
Washenfelder, R. A., A. O. Langford, H. Fuchs, and S. S. Brown (2008), Measurement of glyoxal using an incoherent broadband cavity enhanced absorption spectrometer, *Atmos. Chem. Phys.*, *8*, 7779–7793.
Washenfelder, R. A., et al. (2011), The glyoxal budget and its contribution to organic aerosol for Los Angeles, California, during CalNex 2010, *J. Geophys. Res.*, *116*, D00V02, doi:10.1029/2011JD016314.
Whalley, L. K., M. A. Blitz, M. Desservettaz, P. W. Seakins, and D. E. Heard (2013), Reporting the sensitivity of laser-induced fluorescence instruments used for HO_2 detection to an interference from RO_2 radicals and introducing a novel approach that enables HO_2 and certain RO_2 types to be selectively measured, *Atmos. Meas. Tech.*, *6*, 3425–3440.
Williams, E. J., D. D. Parrish, M. P. Buhr, F. C. Fehsenfeld, and R. Fall (1988), Measurement of soil NOx emissions in Central Pennsylvania, *J. Geophys. Res.*, *93*, 9539–9546.
Wong, K. W., C. Tsai, B. Lefer, C. Haman, N. Grossberg, W. H. Brune, X. Ren, W. Luke, and J. Stutz (2012), Daytime HONO vertical gradients during SHARP 2009 in Houston, TX, *Atmos. Chem. Phys.*, *12*, 635–652, doi:10.5194/acp-12-635-2012.
Yarwood, G., T. E. Stoeckenius, J. G. Heiken, and A. M. Dunker (2003), Modeling weekday/weekend ozone differences in the Los Angeles region for 1997, *J. Air Waste Manage.*, *53*, 864–875.
Young, C. J., et al. (2012), Vertically resolved measurements of nighttime radical reservoirs; in Los Angeles and their contribution to the urban radical budget, *Environ. Sci. Technol.*, *46*, 10,965–10,973, doi:10.1021/es302206a.